The May 20 (M_W 6.1) and 29 (M_W 6.0), 2012, Emilia (Po Plain, northern Italy) earthquakes: new seismotectonic implications from subsurface geology and high-quality hypocenter location

Simona Carannante [(1)]*, Andrea Argnani [(2)], Marco Massa [(1)], Ezio D'Alema [(1)], Sara Lovati [(1)], Milena Moretti [(3)], Marco Cattaneo [(3)] , Paolo Augliera [(1)]

[(1)] Istituto Nazionale di Geofisica e Vulcanologia (INGV), Sezione Milano, via Edoardo Bassini 15, 20133 Milano, Italy.

[(2)] Istituto di Geologia Marina (CNR-ISMAR), Via Gobetti 101, 40129 Bologna, Italy.

[(3)] Istituto Nazionale di Geofisica e Vulcanologia (INGV), Centro Nazionale Terremoti, via di Vigna Murata, 00143 Roma, Italy.

Revised version: May 2015

***Corresponding author: Simona Carannante**

Istituto Nazionale di Geofisica e Vulcanologia (INGV)

Sezione Milano

via Edoardo Bassini 15

20133 Milano, Italy

Email: simona.carannante@ingv.it

Abstract

This study presents new geological and seismological data that are used to assess the seismic hazard of a sector of the Po Plain (northern Italy), a large alluvial basin hit by two strong earthquakes on May 20 (Mw 6.1) and May 29 (Mw 6.0), 2012. The proposed interpretation is based on high-quality relocation of 5,369 earthquakes ('Emilia sequence') and a dense grid of seismic profiles and exploration wells. The analysed seismicity was recorded by 44 seismic stations, and initially used to calibrate new one-dimensional and three-dimensional local Vp and Vs velocity models for the area. Considering these new models, the initial sparse hypocenters were then relocated in absolute mode and adjusted using the double-difference relative location algorithm. These data define a seismicity that is elongated in the W-NW to E-SE directions. The aftershocks of the May 20 mainshock appear to be distributed on a rupture surface that dips ~45° SSW, and the surface projection indicates an area ~10 km wide and 23 km long. The aftershocks of the May 29 mainshock followed a steep rupture surface that is well constrained within the investigated volume, whereby the surface projection of the blind source indicates an area ~6 km wide and 33 km long. Multichannel seismic profiles highlight the presence of relevant lateral variations in the structural style of the Ferrara folds that developed during the Pliocene and Pleistocene. There is also evidence of a Mesozoic extensional fault system in the Ferrara arc, with faults that in places have been seismically reactivated. These geological and seismological observations suggest that the 2012 Emilia earthquakes were related to ruptures along blind fault surfaces that are not part of the Pliocene-Pleistocene structural system, but are instead related to a deeper system that is itself closely related to re-activation of a Mesozoic extensional fault system.

Keywords: velocity model, relocated hypocenters, double-difference locations, Po Plain, blind faults, May 2012 Emilia earthquakes, reactivated extensional faults

Introduction

The Po Plain (northern Italy) is a large alluvial plain located in the foreland of two opposite-verging fold-and-thrust belts, the Northern Apennines and the Southern Alps (e.g., Fantoni and Franciosi, 2010). As common for other large and tectonically active alluvial basins, the Po Plain is characterized by relevant blind faulting. The issue of blind faulting became widely debated in the Earth sciences community in 1989, following publication of details of a sequence of 'hidden earthquakes' that hit central and southern California, USA, between 1983 and 1987, and following the October 17, 1989, Loma Prieta earthquake (MW 6.9) in northern California, USA (Burrato et al., 2012). Stein and Yeats (1989) indicated clearly that *"large earthquakes can take place not only on faults that cut the Earth's surface, but also on 'blind' faults under folded terrain*".

This debate found a practical example on May 20, 2012, when at 02:03:52 UTC, a Mw 6.1 earthquake (hereinafter the *Emilia earthquake*, Scognamiglio et al., 2012; Luzi et al., 2013) occurred in the central part of the Po plain tectonic domain (northern Italy). This area, below the Plio-Quaternary sedimentary cover is characterized by an arcuate thrust system and related growth folds (Pieri and Groppi, 1981; Pieri, 1983). The May 20 mainshock was followed by six severe aftershocks with $M_L \geq 5$ (Fig. 1a), the strongest of which was Mw 6.0, and occurred on May 29, 2012, at 07:00:03 UTC.

Considering the instrumental seismicity recorded from 1983 to May 20, 2012 (Fig. 2a), the study area has been hit by only three low to moderate earthquakes (INGV Instrumental Bulletin, http://bollettinosimico.rm.ingv.it): the December 6, 1986, Polesine earthquake (ML 4.1; Fig. 2a, #1), the May 8, 1987, Mantova earthquake (ML 4.0; Fig. 2a, #2), and the July 17, 2011, Ferrara earthquake (ML 4.7; Fig. 2a, #3). The historical information reported in the CPTI11 catalog (Rovida et al., 2011) illustrate that the major events were the earthquakes of: March 20, 1234 (Mw 5.17; Io 7.0; Fig. 2b, #3), February 22, 1346 (Mw 5.81;

Io 7.5; Fig. 2b, #1), November 17, 1570 (Mw 5.48; Io 7.5; Fig. 2b, #4), and March 17, 1574 (Mw 5.12; Io 7.0; Fig. 2b, #2).

Also considering these data, it is evident that at the Italian scale, the investigated area is characterized by moderate values of seismic hazard, with maximum expected horizontal peak ground accelerations (calculated for rock-site conditions, with a return period of 475 years; Stucchi et al 2011) in the range of 0.125 *g* to 0.175 *g*. Nevertheless, during the May 20 mainshock, important discrepancies between the official Italian seismic hazard map and the recorded ground motions (acceleration up to ~0.3 *g*) were observed. As reported by Stucchi et al. (2012), one of the possible causes is the soil conditions of the Po alluvial basin. As recently demonstrated by Luzi et al. (2013), the structure of the Po plain can 'trap' the incoming direct wavefield and convert the body waves into surface waves, thus producing both relevant ground shaking (also at long period; Massa et al., 2013) and longer duration. This behavior has also been observed and simulated for other important alluvial basins worldwide, such as for Los Angeles Basin, USA (Hanks, 1975; Joyner, 2000; Somerville et al., 2004), Osaka Basin, Japan (Kagawa et al., 2004), and Kanto Basin beneath the city of Tokyo, Japan (Hisada et al., 1993; Sato et al., 1999).

Merging together the information reported above and considering the wide exposure of the area, and in some cases the moderate degree of vulnerability, it is clear that the Po Plain represents an area of high seismic risk. Indeed, the 20 casualties and the €5 billion damage produced by the May 20 earthquake attest to this.

In this kind of seismotectonic setting, detailed knowledge of the blind faults that are potentially seismogenic is a very important issue. In recent years, many studies have debated the tectonic evolution of the Northern Apennine thrust front and the Po Plain foredeep, to try to outline the structural style of the mountain front and to characterize the tectonic activity of the folds buried beneath the subsurface of the Po Plain (Fantoni and Franciosi, 2008, 2010;

Picotti and Pazzaglia 2008; Toscani et al., 2009; Boccaletti et al., 2011). Some studies have supported the hypothesis that the tectonic activity of the frontal part of the Northern Apennines stopped in the Early Pleistocene (Argnani et al., 1997; Bertotti et al., 1997; Argnani et al., 2003; Picotti and Pazzaglia 2008). Other studies, instead, have suggest that some of the anticlinal structures buried in the Po Plain are still tectonically active, on the basis of geomorphological and subsidence analysis (Burrato et al., 2003; Scrocca et al., 2007).

The 2012 seismic sequence offered a chance to investigate the active fault system and to review the different tectonic interpretations of the thrusts and folds of the Ferrara Arc. This has resulted in several studies based on comparisons between the new seismic data collected during the Emilia sequence (mainshocks and aftershocks) and the sub-surface geological structures and geomorphological evidence (e.g., Malagnini et al., 2012; Burrato et al., 2012; Ventura and Digiovanbattista, 2013; Bonini et al., 2014). Other studies have provided new models of faults and displacement patterns through inversion of geodetic data (Pezzo et al., 2013; Tizzani et al., 2013) and through tomographic inversion methods and/or relocated seismicity (Govoni et., 2014; Chiarabba et al., 2014).

The present study provides a new hypothesis that we have developed in the framework of the 2012-2013 INGV-DPC S1 Seismologic Project (https://sites.google.com/site/ingvdpcs1project/). In this study, through the availability of seismicity data from more than 5,000 earthquakes, and to a dense grid of multichannel seismic profiles and exploration wells, we present a model that consistently accounts for the 2012 seismicity and for the regional evidence of active tectonics. Unlike other recent contributions which have assumed continuing deformation along the geological structures formed in the Pliocene (Malagnini et al., 2012; Burrato et al., 2012; Lavecchia et al., 2012; Ventura and Digiovanbattista, 2013; Bonini et al. 2014; Govoni et al., 2014), we show that a relevant role is played by pre-existing and reactivated extensional faults that appear to be of

Mesozoic age. A partly similar conclusion was presented recently by Chiarabba et al. (2014), even if there is difficulty, in our opinion, for the co-existence of thin-skinned and thick-skinned active deformation that was proposed to be consistent with the regional tectonic framework.

Geological settings

The Po Plain is one of the largest alluvial basins on the global scale. It is characterized by an area of ~50,000 km^2 (map extension: ~350 km longitudinally, ~150 km transversally) and a thickness of Pliocene-Quaternary clastic sediment that varies from hundreds of meters to ~7 km (Pieri and Groppi, 1981). The basin is bordered to the north by the Southern Alps and to the south by the Northern Apennine mountain range. Although the Po Plain has a flat appearance, early hydrocarbon exploration revealed that the frontal thrusts of the Apennines are buried underneath a thick layer of clastic sediments (Pieri and Groppi, 1981). This buried Apennines thrust front has formed a series of three asymmetric arcs, and from west to east, these have been named as the Monferrato, Emilia and Ferrara Arcs (Fig. 1b).

The occurrence of this arcuate thrust front is somewhat at odds with the straight line that outlines the *pede*-Apennines, and so it represents a structural arrangement that suggests some control from inherited features in the foreland (Argnani and Frugoni, 1997). The increasing availability of good quality seismic profiles that have been calibrated by exploration wells has allowed regional cross-sections to be drawn through these buried arcs (e.g., Fantoni and Franciosi, 2010), which were formed mainly from the Early Pliocene to the Middle Pleistocene (Ghielmi et al., 2010). These cross-sections showed that Mesozoic carbonate units were involved in the thrust sheets that formed the Ferrara Arc, unlike the arcs to the west, where only the Cenozoic clastic sediments were involved (Pieri and Groppi, 1981; Fantoni and Franciosi, 2010). The thickness of the Pliocene-Quaternary sediment that

fills the Po Plain foredeep basin is great (up to 8 km), making it difficult to image the deeper parts of the thrust system on seismic profiles. This might partly explain the different interpretations of the Ferrara Arc in the literature, where the basement is sometimes involved (e.g., Picotti and Pazzaglia, 2008) and sometimes not (e.g., Carminati et al., 2010). The role of the basement is relevant to the issues of earthquake faulting and of re-activated, inherited structures.

The long-term evolution of the foredeep system indicates a remarkable north-eastward migration of the thrust front, which decreased after the Middle Pliocene (Argnani and Ricci Lucchi, 2001). GPS velocities have also indicated that convergence is currently limited across the Po Plain, with the larger gradient just at the *pede*-Apennines (Bennett et al., 2012) The low strain and the large sedimentation rate make it difficult to determine whether the buried thrust fronts are active or not, and also because the industrial seismic profiles often lack the resolution to image the geometry of the most recent sediments. Late Pleistocene deformation has clearly been occurring at the *pede*-Apennines, which suggests that most of the current convergence can be accommodated here, whereas the growth strata related to the buried outer structures indicate that there was little or no deformation by the Late Pleistocene (e.g., Argnani and Frugoni, 1997; Picotti and Pazzaglia, 2008). Other studies, however, have indicated that the buried arcs are also active, although with very low deformation rates (e.g., Scrocca et al., 2007), and they have possibly affected the evolution of the rivers (Burrato et al., 2003).

Before the Emilia 2012 earthquakes, the only record of relevant seismicity was for the Ferrara 1570 earthquake. Indeed, the instrumental seismicity had been very limited, with earthquakes that were mostly located in the middle-lower crust (Chiarabba et al., 2005). The Emilia 2012 sequence occurred to the west of this historical Ferrara earthquake (CPTI11, Rovida et al., 2011), which suggests that the Ferrara Arc is seismogenic. A question that will

be addressed here relates to the geometry of the seismogenic faults, which is defined by the accurate three-dimensional (3D) hypocentral relocations presented here. In particular, a point of major relevance is to understand whether the seismogenic faults are the same as the thrust faults that originated the outer arcs, or whether they represent new features, which might be controlled by the Mesozoic structural inheritance.

Earthquake datasets and data processing

On May 20, 2012, at 02:03:52 UTC, an earthquake with M_W 6.1 (European-Mediterranean Regional Centroid-Moment Tensors Catalog: http://www.bo.ingv.it/RCMT/) hit the central part of the Po Plain, in particular in the area around the towns of Modena, Mantova and Ferrara (Fig. 1). This mainshock was followed a few hours later by three severe aftershocks that had very similar epicenters and ML of 4.8, 5.1 and 4.9, and by thousands of smaller aftershocks. Nine days later, on May 29, at 07:00:03 UTC, a further strong event with MW 6.0 (European-Mediterranean Regional Centroid-Moment Tensors Catalog: http://www.bo.ingv.it/RCMT/) occurred ~15 km west of the first mainshock. This second mainshock was also followed by thousands of aftershocks, the strongest of which had ML 5.3, 5.2 and 5.1. The month of June 2012 was then characterized by a progressive decrease in the seismic rate and seismic moment release.

The data used in the present study were recorded by a total of 44 *Istituto Nazionale di Geofisica e Vulcanologia* (INGV; National Institute of Geophysics and Volcanology) seismic stations (Table 1). These stations were both permanent (i.e., RSN, National Seismic Network; Amato and Mele, 2008), which were selected for a maximum epicentral distance of 100 km, and temporary, which were installed in the epicentral area after the May 20 mainshock (Moretti et al., 2012). Due to the new installations, the average inter-station distance was decreased from ~30 km to 8 km.

To collect the dataset necessary to calibrate the velocity model that can be used to relocate the available hypocenters, the data recorded from May 18 to July 3, 2012, were considered. In this way, thousands of earthquakes with ML from 1.0 to 5.9 (i.e., the May 20 mainshock) were selected from the continuous recorded signals using an automatic procedure developed by Marzorati et al. (2012), and based on the short time average (STA)/ long time average (LTA) algorithm (Borman, 2012). In particular, the STA and LTA windows were set to 1 s and 50 s, respectively, while the coincidences (i.e., the events detected by more than an a-priori established number of receivers) were calculated considering a 20-s windows with a shift of 5 s. After the trigger detection, the earthquakes were selected from the continuous MiniSeed format (Standard for the Exchange of Earthquake Data, SEED; http://www.iris.edu/dms/nodes/dmc/data/formats/) with the assumption of a pre-event window of 20 s and a post-event window of 60 s. Finally, the selected data were converted into SAC binary format (www.iris.edu/software/sac/manual/file_format.html).

After the preprocessing step, to delete false events detected by the automatic procedure, all events was analyzed using the SacPicker code, developed by Spallarossa et al. (2011). In this way, 5,369 earthquakes were collected, for a total of of 60,832 P-wave arrival times and 52,757 S-wave arrival times. It is important to note that all of the events with ML $\geq$3.0 were checked again and hand-picked later.

With respect to the INGV bulletin that soon after the sequence localized about 2,150 hypocenters (http://iside.rm.ingv.it), we identified 3,194 new earthquakes. In particular, 69 new events with ML from 2.5 to 3.0 and three new events with ML from 3.0 to 3.5 were detected. For the lower magnitude events, we identified 240 new events with ML <1, 2,789 with 1 $\leq$ML <2.0, and 93 with 2.0 $\leq$ML <2.4.

Overall, the available dataset allowed us to work using a number of events (and detected phases) that were double those used in the recent report in the same issue (e.g.,

Govoni et al., 2014; Chiarabba et al, 2014). In particular, the higher number of data allowed us to reliable investigate depths up to about 15 km.

To obtain a preliminary location, all of the available travel-times were inverted using the Hypo-Ellipse code (Lahr, 1979), which included the simple one-dimensional (1D) three-layer velocity model used by the INGV for the first locations (D'Alessandro et al., 2010).

One-dimensional and three-dimensional local velocity models

To investigate the 3D structural variations of the area, reliable earthquake locations are required. The initial and fundamental condition for useful 3D seismic wavefield propagation models is a dense network installed around a cloud of seismicity that is characterized by a geometry that assures good azimuthal coverage (Carannante et al., 2012). Considering the high number of available seismic phases, as described in the previous paragraph (5,369 events, 60,832 and 52,757 P and S-wave arrival times, respectively), and the optimal coverage of the seismic stations installed in the epicentral area (Fig. 1), a quality subset of 650 earthquakes was selected to calculate both the stable 1D and 3D velocity models. Without imposing condition on root mean square (rms) values and considering the data with a maximum azimuth gap of 150° and a minimum number of seismic phases of 20, the final result of our selection was a set of 650 events with a mean rms of 0.28 s and mean erh (horizontal location error) and erz (vertical location error) of 0.83 km and 1.11 km, respectively (Fig. 3a).

In the velocity model calibration, a very important step is represented by a good trade-off of the available ray paths with respect the investigated selected volume. To balance the ray-path coverage well, and as also performed by Govoni et al. (2014), we at first portioned the area into a 3D sub-volume of 3.5 km, both in extent and depth, and then we selected a maximum number of 10 hypocenters inside each seismogenic volume.

The velocity model was calculated by computation of the local earthquake tomography using the Simulps14 code (Thurber, 1983, 1993; Eberhart-Phillips, 1986; Haslinger, 1998). The procedure consists of an iterative damped least-squares inversion that minimizes the residuals between the observed and computed arrival times, to simultaneously solve the Vp and Vp/Vs, and provide the hypocentral determination for each node of the 3D grid.

At first, a new 1D local velocity model was calibrated for the above-mentioned high-quality subset of 650 earthquakes, with the starting point of the 1D velocity model that was calibrated for the area by Ciaccio and Chiarabba (2002). The new 1D Vp model was obtained with a variance reduction of 46% with respect to the starting model, and a final weighted rms of 0.229 s. The data were also inverted to obtain the Vp/Vs ratios and the related Vs model (Fig. 3b).

The 3D inversion was then performed using this minimum 1D velocity model and the same high-quality hypocenter dataset of 650 events described above. An approximate 3D ray-tracing technique was used (Um and Thurber, 1987), which can produce curved non-planar ray paths. With the damping for station delays included (which are sometimes not taken into account in tomography inversions), the damping parameters were empirically chosen by evaluation of the trade-off between the data and the model variance. The choice of damping is quite critical in the inversion problem (Kissling et al., 2001) as it affects both the results and this resolution, and in this case, indirectly, also the event locations. Finally, we set the damping values to 60, 120 and 300, for the Vp, Vp/Vs model and station correction, respectively. The volume of the analyzed area, which was ~90 km wide in both the NS and EW directions (with respect the barycenter of the sequence), was subdivided in depth according to nine non-equally spaced layers from 0 km to 80 km; only the first five layers were equally spaced at 4 km in the vertical direction, while the last deeper layer was chosen

above for the issue of the stability of the inversion. In the horizontal planes, we chose a grid with cells of 5 km × 5 km. After six iterations, a suitable 3D model was obtained, with a variance reduction of 67% and a final weighted rms of 0.17 s. Both rms and variance reduction values are comparable with those recently obtained by Chiarabba et al. (2014), at 0.17 s and 76%, respectively.

At the end of these iterations, and considering that the basic role of the velocity model is to obtain accurate earthquake locations, resolution analysis was also computed. The assessment of the solution quality was mostly estimated by analysis of the resolution matrix (i.e., a squared matrix where each row describes the dependence of one model parameter on all of the other parameters of the model), in terms of the derivative-weighted sum and resolution diagonal element distributions. The Derivative-Weighted Sum (DWS) is the total weighted ray length in each cell, and it provides a measure of the ray density, while the resolution matrix diagonal elements (RDE) lie in the range of 0 to 1 and provide information about the resolved nodes (0, no resolution; 1, perfect resolution). The analysis of the derivative-weighted sum distributions was useful to evaluate the grid parameterization during the algorithm calibration stage. The resolution diagonal element and the derivative-weighted sum distributions (Fig. 4a, b, respectively) showed high values in the central part of the analyzed area (RDE range, 0.7 to 0.9), in particular for layers at 4 km (depths between 2 km and 6 km), 8 km (depths between 6 km and 10 km) and 12 km (depths between 10 km and 14 km), where the bulk of the seismicity was concentrated (including the May 20 and 29 mainshocks). However, also considering the layer at 16 km (depths between 14 km and 18 km), both the RDE and DWS are shown as that the model is well solved in the center of the seismic area, even though, as expected, the lower number of ray coverage slightly affected the possible resolution.

For further information, a spread function (SF) analysis for the Vp and Vp/Vs models

was also performed. The SF is defined as the sum of elements of the resolution matrix weighted by the distance to the corresponding diagonal elements, and it gives additional information on the model resolution. As no information comes from the SF about spatial smearing, usually a 70% smearing contour is plotted for the node, with a relatively low SF (in this case, 2.0). For brevity, Figure 5 only shows the results in the layers for the Vp model: as expected, especially for the layer with a depth between 4 km and 2 km, well-resolved nodes were characterized by low SF (≤1.5 black contouring; ≤ 2.0 gray contouring) and very low to null smearing, in particular in the central area where the May 20 and May 29 mainshocks are located (Fig. 5, red stars on 4 km and 8 km layers, orange stars on 12 km and 16 km layers).This is sufficiently accurate for the deeper layer at 16 km, where in spite of the moderately higher SF, in some areas low smearing was still evident. The resolution analysis appears to be in good agreement with that of Chiarabba et al. (2014), even though the lack of the 15 km depth did not allow a complete comparison.

In Figure 6a, the final P-wave velocity model expressed as absolute values is show in correspondence with the well-solved shallower layers; Figure 6b shows the related Vp/Vs ratio. Although a complete discussion of this model is beyond the scope of this report, it is interesting to indicate the good correlation between the high-velocity and low-velocity anomalies of the shallower layers, and the well-known structures inferred for the area by the geological subsurface data (Fig. 6a, red and green lines from Bigi et al., 1991 and Boccaletti et al., 2004). In particular, the low velocity volumes (Vp ~3 km/s) that are evident between 0 km and 4 km (Fig. 4a) should be related to the deep synclines of the thrust-fold systems and the presence of the Pliocene-Pleistocene sediments (Ciaccio and Chiarabba, 2002; Chiarabba et al., 2014). Conversely, the high Vp (Vp ~4.5-5.0 km/s) that is more evident at 8 km follows the anticline structure of the Mesozoic carbonate (Fig. 6a). These values appear to be in good agreement with those obtained recently by Chiarabba et al. (2014), who for the highest

velocity anomalies (Vp ~6 km) in corrispondence with the extremely high Vp/Vs anomalies in particular, suggested the presence of Mesozoic fluid-saturated carbonates,. For the deeper layers (Fig. 6a, 12-16 km), the preferential wavefield propagation toward the north with respect to the Apennines front (i.e., the Alpine crust) is evident, and it is probably associated with the complexity of the basement.

Absolute hypocenter relocation

The 3D P-wave and S-wave propagation models were used to perform the absolute relocation of the available events. The new coordinates were determined, again using the Simulps14 code. Finally, 5,369 earthquakes were relocated, 736 of which had M_L from 2.5 to 5.9, and 4,633 with M_L <2.49. The events with a depth <1 km and >30 km were considered as outliers and were removed from the final dataset. Figure 7 shows the goodness of the final absolute locations (gray bars) in terms of the rms, which on average is <0.25 s, and both the horizontal (erh) and vertical (erz) location errors, both of which are on average <400 m. In general, the events characterized by at least 25 available seismic phases were localized with rms <0.15 s, while the data with the number of seismic phases ranging between 15 and 25 show the final rms between 0.15 s and 0.30 s. Figure 8 highlights the improvements assured by the new absolute location (dark green symbols) with respect to the initial INGV routine locations (~2,150 events, light gray symbols), as provided by the Italian Seismological Instrumental and Parametric database (http://iside.rm.ingv.it) soon after the occurrence of the Emilia sequence. The direction of the eight cross-sections was fixed perpendicular to the strike of the May 20 mainshock, as inferred by the INGV focal mechanism that was computed through the time-domain moment tensor (http://cnt.rm.ingv.it/tdmt.html).

The map projection of Figure 8a indicates in particular the sparse seismicity pattern produced by the initial INGV routine locations, while for the depth (Fig. 5b), the evident false

alignments of the hypocenters around 5 km and 10 km are the consequence of the three-layer INGV velocity model used during the routine first locations (D'Alessandro et al., 2010).

The new locations of the seven earthquakes with with ML >5 are shown in Figure 8 in the dark yellow and red symbols (the May 20 and 29 mainshocks). While considering the cloud of seismicity related to the May 20 sequence (Fig. 8, sections 5 to 8), the data are in good agreement with those reported in recently published studies (e.g., Govoni et al., 2014; Chiarabba et al., 2014), and it is important to note that concerning the May 29 sequence, in general, we obtain deeper hypocenters (up to ~15 km). In particular, the May 29, 2012, mainshock hypocenter was moved from ~10 km to ~13 km. Considering both the results of the statistical procedure used to validate the proposed velocity models (Figs. 4, 5) and the subsequent goodness of the location process (Fig. 7), it is possible to consider the proposed locations as fully reliable. The slight differences with respect to the previous study might have arisen, in our opinion, from the important differences in terms of the available initial data: our dataset included a number of earthquakes double those with respect to the recently published studies, with a direct first impact in the strength of the velocity models than those used to relocate the selected seismicity.

Figure 9 shows the epicenters and hypocenters (drawn with different colors) as functions of the time of their occurrence, to clearly highlight the migration pattern of the seismicity. The Emilia seismic sequence started around May 18, 2012, due to the activation of the blind fault segment that generated the first mainshock of May 20, 2012 (M_L 5.9; M_W 6.1). As can be seen from the gray symbols in section 5 of Figure 7, the mainshock breaks the volume that included the hypocenters of the weak foreshocks that occurred in the area from May 18 to 20 (time <02:03:52 UTC). The May 20 mainshock coincided with a low-angle fault segment (~45°) that dipped toward the S-SW.

Over the following 3 days after May 20, the seismicity migrated east of the mainshock hypocenter. In particular, two other earthquakes of M_L 5.1 occurred in the eastern sector (Fig. 7, sections 7, 8) of the fault plane that generated the mainshock (i.e., Fig. 7, sections 5 to 8). Over the same period, a further seven moderate seismic events with M_L from 4.2 to 4.9 occurred in the same area. In the period from May 23 to 28, the seismicity pattern began to cover a wider volume, both east and west to the May 20 mainshock.

On May 29, 2012 (07:00:03 UTC), the second mainshock of M_L 5.8 (M_W 6.0) broke a different sector of the blind faults of the area. In this case, the fault plain was localized west with respect to the May 20 seismic source, and it showed a more vertical plane (~70°), and also in this case, it dipped toward the S-SW. After the second mainshock, the seismicity clearly moved toward the west. On the same day, there were a further two strong aftershocks of M_L 5.3 and 5.2 on the related fault segment (i.e., Fig. 7, sections 1 to 4), along with three moderate events with M_L from 4.2 to 4.7 (Fig. 7, section 2). Over the following days, there were several earthquakes generated on the same fault plane, the strongest of which (M_L 5.1) occurred on June 3, 2012 (Fig. 7, section 2). After June 10, 2012, both the seismic energy release and the rate of seismicity strongly decreased.

Relative locations

Seismicity analysis for the study of tectonic processes, earthquake recurrence, and earthquake interactions requires knowledge of the precise spatial offset between the earthquake hypocenters. As has been demonstrated, the accuracy of routine absolute locations is dependent on several factors, which include network geometry, available seismic phases, arrival-time accuracy, and knowledge of the crustal structure (e.g., Poupinet et al., 1984; Fremont and Malone, 1987; Gomberg et al., 1990; Got et al., 1994; Cattaneo at al., 1997; Waldhauser and Ellsworth, 2000; Massa et al., 2006; Marzorati et al., 2013). In the present

study, to overcome possible residual uncertainties in the absolute locations, and with the aim to better define the possible geometry of the investigated seismic sources, the relative locations of the hypocenters were finally computed based on the double-difference algorithm (Waldhauser and Ellsworth, 2000). This technique treats every member earthquake as a master event, and finds a consistent master-slave relationship for a complete catalog in terms of the relative locations of the hypocenters. This uses the HypoDD code (Waldhauser 2001), and allows simultaneous relocation of large numbers of earthquakes over a large distance, including ordinary absolute travel-time measurements and/or cross-correlation P-wave and S-wave differential travel-time measurements (although these were not available in our case). The residuals between the observed and theoretical travel-time differences (i.e. the double differences) are minimized for the pairs of earthquakes at each station, linking together all of the observed event-station pairs.

The double-difference equation that defines the residual is given by:

$$dr^{ij}_k = (t^i_k - t^j_k)^{obs} - (t^i_k - t^j_k)^{cal} \qquad (1),$$

where dr^{ij}_k is the residual between the observed and calculated differential travel-times between two events, the term $(t^i_k - t^j_k)^{obs}$ is the observed travel-time difference between the events i and j recorded at k station, and the term $(t^i_k - t^j_k)^{cal}$ is the calculated travel-time difference between these same events. A least-squares solution was found by iteratively adjusting the vector difference between hypocentral pairs. In the present case, only ordinary absolute travel-times derived from the relocated dataset were used. In particular, both the P-wave and S-wave phase measurements recorded by all of the INGV stations were taken into account.

The reliability of our relative relocations is assured by the geometry of the available

seismic stations with respect to the relocated hypocenters (Fig. 1a). Indeed, as demonstrated by Michelini and Lomax (2004), to avoid artifacts in the relative positions of the hypocenters determined by a double-difference code, accurate knowledge of the velocity structure of the area is necessary. In the double-difference method (Waldhauser and Ellsworth, 2000), the mapping matrix is composed of partial derivatives of the travel-times with respect to the hypocenter coordinates, which are directly related to the take-off angles of the rays that connect the foci and the receivers. Thus, the inverse mapping of the double-difference data into perturbations in relative locations of the event hypocenters and their origin times is controlled by the ray take-off directions at the hypocenters. As a consequence, if the ray directions are different from the true ray directions, it is possible that the information in the residual travel-time double differences will be mapped incorrectly into hypocenter perturbations, which will bias the data (Michelini and Lomax, 2004).

The relative locations are shown in Figure 8 (black symbols) and these were computed just considering ~1,300 hypocenters that were relocated with final rms ≤0.15 s (minimum number of phases, 25). Considering that at present the HypoDD code cannot be used to implement the 3D velocity model, the 1D velocity model shown in Figure 3 was used as the input to relatively locate the selected events. The black symbols in Figure 8 show the presence of two separate fault segments better: the eastern segment (May 20 mainshock; M_W 6.1) is characterized by a lower dipping angle in a SW direction (Fig. 8a, sections 5 to 8), while the western segment (May 29 mainshock; M_W 6.0) shows a more vertical seismicity pattern in the same dipping direction, and in particular in the central part of the blind fault plane (Fig. 8a, sections 3, 4).

Seismotectonics interpretation

With the combination of the data presented in the previous paragraph with the information coming from the available dense grid of commercial multichannel seismic profiles, a new interpretation is presented to account for the geological structures, the timing of the deformation, and the relationships with the relocated earthquakes of the Emilia 2012 sequence. In particular, the commercial multichannel seismic profiles that were kindly made available by ENI (*Ente Nazionale Idrocarburi*) allowed us to outline the subsurface geology of the Ferrara Arc (Fig. 1b). The available profiles were interpreted using the seismic stratigraphy approach (Payton, 1977). The seismo-stratigraphic units were subsequently tied to the stratigraphy obtained from exploration wells. Particular attention was given to highlight the sedimentary record of the deformation, such as the growth strata (Shaw and Suppe, 1994). Seismic interpretation has shown the occurrence of extensional faults that pre-exist the Pliocene thrusting (Fig. 10a, top panel). These faults appear to belong to a Mesozoic extensional system that affected the Adria domain, although some of them might have been re-activated during the flexure of the Adria plate in front of the advancing Apennine belt. These extensional faults are more evident in the area west of Ferrara (Fig. 10a, top panel), where they were reported also in initial subsurface investigations (e.g., Pieri and Groppi, 1981). The most relevant of these extensional faults, however, extends from Reggio Emilia to Ferrara, and appears to have controlled the development of the Mirandola Arc (Fig. 10a, top panel).

Three seismic lines that cross the Ferrara Arc are used to present the geological interpretation (Fig. 10, top panel). Some of the key features are best expressed in the profile that crosses the lateral ramp of the Ferrara Arc (just west of the epicenters of the Emilia 2012 earthquakes), where there is little complexity (Fig. 10, section ‘a’). The structure appears as a simple fault-related fold, where the thrust ramp is controlled by an extensional fault in the

Mesozoic units, which is evident as a marked step. The growth strata suggest that folding mainly occurred within the middle-late Pliocene, before the deposition of the Po Plain prograding unit (Ghielmi et al., 2010, 2013), which spanned the Middle Pleistocene. This unit can be traced all over the Po Plain, where it often presents a prograding reflection geometry, and it was deposited between ~0.9 Ma and 0.6 Ma. In the seismic profile, the reflections of this unit are subparallel and onlap the top of the ramp anticline, which is marked by a truncated surface. This observation is taken as an indication that the folding ceased during the deposition of the Po Plain prograding unit. The strata package that defines the Po Plain prograding unit is slightly folded above the anticline, but with a wavelength that is larger than that of the anticline. This suggests that a deeper fault is responsible for the mild and large wavelength folding. We thus infer that the Mesozoic extensional fault at the bottom of the seismic profile was re-activated in a reverse sense. As well as accounting for the folding of the Po Plain prograding unit, this interpretation also suggests that deeper units were recently involved in the deformation of the outer Apennine fronts. The same features, although with some variation, can be observed in the seismic profiles that cross the area of the May 20 and 29, 2012, earthquakes.

Line ‘b’ in Figure 10 shows the seismic profile that crosses the frontal ramp of the Ferrara Arc in the area of the May 29 earthquake. This shows a very large step in the lower part of the profile that is defined by the regional trend of the Mesozoic carbonate reflectors. The step is inferred to be related to a Mesozoic extensional fault, which controls the thrust ramp of the Mirandola anticline. This Mesozoic extensional fault can be mapped westward to join the step observed in the previous profile, and eastward to continue for over 20 km, toward Ferrara (Fig. 10a, top panel).

We have converted the relocated hypocentral depths of the May 29 seismic sequence into a two-way travel-time (TWT), to locate the earthquakes on the time-migrated seismic

profile. In Figure 10b, black and gray circles (hypocenters relocated with rms ≤0.15 s and 0.30 s, respectively) superimposed to seismic profile 'b' are the results of the hypocentral depths converted to TWT. For the TWT conversion, we used the velocity log of confidential data from a deep well located west of Ferrara, which was complemented with the velocity data for the basement units (Patacca et al., 2008). We adopted this procedure because we prefer to maintain the geometry observed on the seismic profiles, instead of depth-converting the profile on the assumption of an mean interval velocity for units that are often located at different depths and might be internally heterogeneous.

It is worth mentioning that the hypocentral depths converted to TWT were previously determined using the velocity models obtained through the tomographic inversion as input. In this way, to check the reliability of the conversion, we first calculate and then compare the TWT obtained by applying both the commercial velocity log and the velocity data obtained in this study. The middle panel of Figure 10a shows the results of our test: the blue and gray symbols represent the results of the conversion using the commercial log and our velocity model, respectively. For both models, in correspondence to each converted hypocenter, the location error (Fig. 7), also converted into TWT, is associated (Fig. 10a, vertical bars). The meaning of this test is to highlight that the contribution of the location errors, in terms of hypocentral depths, is in any case greater than possible errors introduced in the TWT determination by using different velocity models. The results described above assures, as a consequence, the absence of significant bias in the proposed procedure.

The May 29 seismicity followed the step in the carbonate units relatively closely, whereas it was not located along the thrust faults that were responsible for the Pliocene folding. The Po Plain prograding unit shows subparallel reflections that onlap the flanks of the Mirandola anticline, following the deposition of the growth strata during the Middle Pliocene-early Pleistocene. Again, the Po Plain prograding unit is slightly folded on either side of the

main anticline, as seen in the previous profile, with a wavelength greater than that of the Mirandola anticline. It is worth noting, instead, that the Po Plain prograding unit shows evidence of syndepositional deformation near the *pede*-Apennines, which suggests that deformation during the middle Pliestocene mostly occurred away from the outer thrust front. A similar observation can be extended over most of the Po Plain *pede*-Apennines (Argnani and Frugoni, 1997; Argnani et al., 2003; Picotti and Pazzaglia, 2008).

Line ‘c’ in Figure 10 shows the seismic profile that crosses the frontal ramp of the Ferrara Arc in the area of the May 20 earthquake, and also shows a step in the lower part of the profile. This step is defined by the regional trend of the Mesozoic carbonate reflectors, and is inferred to be related to a Mesozoic extensional fault. Also in this case, we converted the relocated hypocentral depth of the May 20 seismic sequence into a TWT, to locate the earthquakes on the time migrated seismic profile (Fig. 10b, black and gray circles in profile ‘c’). Also in this case, the reliability of the conversion is assured by the same test performed for the May 29 sequence (Fig. 10a, bottom panel).

The May 20 seismicity broadly defines a footwall shortcut trajectory (e.g., Cooper et al., 1989) with respect to the Mesozoic extensional fault. The Po Plain prograding unit shows subparallel reflections that onlap the flanks of the anticlines. This unit is slightly folded at the edge of the two main anticlines, but with a wavelength that is greater than that of the individual anticlines. The gentle fold is roughly located above the shortcut ramp defined by the seismicity.

By comparing the Emilia 2012 hypocentral distribution with the interpretation of the multichannel seismic profiles, some key observations can be established. The main deformation of the Ferrara folds appears to be have been completed by the time of the deposition of the Po Plain prograding unit; i.e., between 0.9 Ma to 0.6 Ma. The hypocentral distribution shows that the seismicity extended below the detachments of the Ferrara Arc fold

system. The limited evidence of deformation that affected the Po Plain prograding unit is observed above a fault ramp that is located below the Pliocene detachment system, with seismicity that closely describes this ramp (Fig. 10b, profile ‘c’). The regional trend of the Mesozoic carbonate units suggests that Mesozoic extensional faults control the location of the contractional ramps. In the case of the May 20 seismic sequence, the distribution of seismicity defined a shortcut fault that was located in the footwall of a Mesozoic extensional fault (Fig. 11). Footwall shortcut faults are typically formed during contractional reactivation of extensional faults (e.g., Cooper et al., 1989), and these can indicate that compression now affects the deeper crustal levels with respect to the Pliocene thrust system (Fig. 12).

Altogether the structures mapped in the Ferrara Arc show a pattern that is consistent with the location of the Emilia 2012 seismicity. During the development of the Pliocene thrust system, the major extensional fault in the area (Fig. 10a, top panel) controlled the location of the main ramp (the Mirandola front) that defines the Ferrara Arc. Since the late Pleistocene, as the deformation affected the deeper crustal levels, some of the Mesozoic faults were re-activated.

In our interpretation the May 20 and 29, 2012, mainshocks nucleate where the limestone units are present, partly in agreement with Chiarabba et al. (2014), whereas the fault ramp can cut deeper into the basement, as also supported by the relocated hypocentral depths (down to ~ 15 km, see figure 8).

Discussion and conclusions

In recent years (before 2012), commercial seismic data were used to construct cross-sections of the Ferrara Arc, with the aim being to outline the structural style of the frontal part of the Apennines (Fantoni and Franciosi, 2008, 2010; Picotti and Pazzaglia, 2008, Boccaletti et al., 2011) or to characterize the tectonic activity of the Po Plain (Toscani et al., 2009;

Carminati et al., 2010). Some of these cross-sections cross the area affected by the 2012 Emilia sequence (Luzi et al., 2013), and these were used for structural reference to relate the tectonics and seismicity of the investigated area. The geological sections can be divided into two main groups. In one group, the basement of the Mesozoic succession was involved in the deformation of the buried thrust fronts (Fantoni et al., 2008, 2010; Picotti and Pazzaglia 2008; Toscani et al., 2009; Boccaleti et al., 2011). In the other group, which is represented by the single cross-section of Carminati et al. (2010), the basement was not involved, and the thrust faults sole out into the Triassic evaporites.

Soon after the earthquakes, the cross-sections from these two groups were extensively used to discuss the seismicity of the Emilia sequence of 2012. The cross-section from the second group has been the most popular (Malagnini et al., 2012; Burrato et al., 2012; Tizzani et al., 2013; Govoni et al., 2014), probably because it lies right across the area of the Emilia sequence. The cross-sections of the first group are not always favorably located with respect to the Emilia sequence, with the exception of the cross-sections of Boccaletti et al. (2011), which have indeed been used for reference in some studies (Pezzo et al., 2013; Govoni et al., 2014). In one instance, a cross-section located outside the area of the Emilia sequence (after Picotti and Pazzaglia, 2008) was used to project the hypocentral seismicity of both the May 20 and 29 sequences, which resulted in a relatively blurred relationship between the seismicity and the fault structures (Ventura and Digiobambattista, 2013).

Despite the different conceptual interpretations of the two groups of sections, they have also been used together in individual studies to frame the structural setting of the earthquake area (Malagnini et al., 2012; Govoni et al., 2014). Moreover, the two seismic sequences of May 20 and 29, 2012, have often been projected onto the same cross-section (e.g., Burrato et al., 2012; Ventura and Digiovanbattista, 2013; Tizzani et al., 2013; Bonini et al., 2014, Chiarabba et al., 2014), although, as shown in the previous section, the structural

style changes remarkably along the strike.

Two new cross-sections were constructed after the 2012 earthquakes. In one case, the basement was involved in the thrust faults that originated the Mirandola and Ferrara folds (Lavecchia et al., 2012); in the other case, the basement was not involved in the Ferrara Arc region, although some short thrust faults that cut the basement were related to the outermost folds (Bonini et al., 2014). It is interesting to note that the traces of the cross-sections presented in the literature are often very close to each other, although the interpretations can differ substantially (e.g., compare Carminati et al., 2010, for the upper Triassic detachment, with Lavecchia et al., 2012, for basement-involved thrusts; and compare Picotti and Pazzaglia, 2008, for the Ferrara thrust detached onto the upper Triassic, with Toscani et al., 2009, for the Ferrara thrust rooted into the basement). This thus illustrates the degree of uncertainty of the data, and how the thrust geometry and depth conversion can depend upon individual interpretation.

One point that is relevant to stress is that all of the structural cross-sections share the view that the thrust system that originated the Ferrara Arc is still active, although with reduced deformation rates. This approach, however, has some problems when the hypocenters of the seismic sequence are considered. The aftershocks of the two relocated sequences of May 20 and 29 (Fig. 8) outline two different fault planes. Even for the routinely located hypocenters, it appears that the rupture planes cut across most of the thrust faults drawn in the cross-sections. This evidence has been interpreted as due to re-activation of multiple thrust planes, with angles that have been shallower with respect to that of the aftershock envelope (Bonini et al., 2014; Govoni et al, 2014). We believe that this interpretation is not consistent with the earthquake rupture, and that it represents an attempt to fit the earthquake rupture within the thrust system that originated the Ferrara Arc in the Pliocene-early Pleistocene.

In the present study, we have presented an alternative seismotectonic interpretation of

the Ferrara Arc based on the analysis of 5,369 earthquakes that occurred during the 2012 Emilia sequence, combined with a large dataset of commercial seismic profiles.

We should note that the very large dataset of seismic events that we relocate (~5,300 earthquakes) allowed us to investigate the distribution of seismicty at greater depth (down to ~15 km). This explains the deeper location of the May 29 mainshock (Fig. 8), compared to previous shallower locations presented in recent studies (e.g. Govoni et al., 2014; Chirarabba et al., 2014). This depth and the fault plane outlined by our robust hypocenters relocation point to a deformation system where the basement is involved. Moreover, due to the accurate relative relocations that were not attempted elsewhere, it was possible to further improve the geometrical setting of the two blind fault planes. The 45º dipping May 20 fault plane strongly suggests a footwall short-cut mechanism when compared to the seismic profiles (Figs. 10, 11).

In our interpretation, we have used seismic profiles located right in the areas of each of the two seismic sequences of the May 20 and 29, 2012 earthquakes. Most importantly, we have mapped the continuity and lateral extent of the structures using subsurface data. Our data lead us to argue that the 2012 Emilia seismic sequence represented the activation of a new and deep-rooted system of deformation within the Adriatic crust (Fig. 12). This contrasts with the conclusions of Chiarabba et al. (2014), who inferred the co-existence of thin-skinned and thick-skinned seismic deformation for the May 29 and May 20 events, respectively.

Arguments in favor of a new deep-seated tectonic system

The three arcs that are buried beneath the Po Plain were formed during the Pliocene-early Pleistocene. However, the limited evidence of seismicity (before the Emilia 2012 sequence; Fig. 2a) and the recent deformation have been observed only in the Ferrara Arc, where the Mesozoic units are involved in the thrust system. For the Emilia and Monferrato Arcs, deformation ceased by the early Pleistocene, and did not progress subsequently (e.g.,

Pieri and Groppi, 1981; Argnani et al., 2003; Ghielmi et al., 2010). On the other hand, deformation occurred throughout the Pleistocene in the *pede*-Apennines, where it appears to be related to deep-seated structures (Argnani and Frugoni, 1997; Picotti and Pazzaglia, 2008).

The involvement of deeper structural levels as deformation progresses is a common observation in continental fold-and-thrust belts (Pfiffner, 2006), as well as in the reactivation of extensional faults located in the foreland of deforming fold-and-thrust belts (e.g., Marshak et al., 2000). The occurrence of Mesozoic extensional faults can be recognized in the seismic profiles of the Ferrara Arc in several cases (Fig. 10). It is here proposed that the occurrence of a Mesozoic extensional system in the Ferrara area favored the involvement of Mesozoic carbonates during the development of the Ferrara folds in the early Pliocene, but also created an inherited weakness that was subsequently exploited when deep structural features along the *pede*-Apennines were activated (or more likely, re-activated). The implication is that the Emilia 2012 seismic sequence, and by inference also the Ferrara 1570 earthquake, was related to activation of a new deformation system that has developed since the late Pleistocene and that affects the deeper structural levels within the Adriatic crust (Fig. 12). This interpretation has major relevance for the seismotectonic characterization of the Po Plain, because the location and extent of the Ferrara folds that were formed during the Pliocene-Pleistocene cannot simply be used to estimate the seismogenic potential of the Ferrara Arc region.

Acknowledgements

The interpretation given in this report stems from the activities carried out by the authors from 2012 to 2013 within the DPC-INGV S1 Project (Base-knowledge improvement for assessing the seismogenic potential of Italy). ENI E&P is gratefully acknowledged for allowing access to their confidential seismic data of the Po Plain. Also A. L. Cazzola, G. Lanfranchi and C. Cattaneo, in particular, were all very helpful. D. Slejko and an anonymous reviewer greatly helped us to improve the manuscript.

References

Amato, A., Mele, F. M., 2008. Performance of the INGV National Seismic Network from 1997 to 2007. Annals of Geophysics, 51, 417-431.

Argnani, A., Frugoni, F., 1997. Foreland Deformation in the Central Adriatic and its Bearing on the Evolution of the Northern Apennines. Annals of Geophysics, 40, 771-780.

Argnani, A., Ricci Lucchi, F., 2001. Terziary silicoclastic turbidite systems of the Northern Apennines. In: Vai, G.B., Martini, I.P. (Eds.), Anatomy of an Orogen: the Apennines and adjacent Mediterranean basins. Kluwer Academic Publishers, 327-350.

Argnani, A., Barbacini, G., Bernini, M., Camurri, F., Ghielmi, M., Papani, G., Rizzini, F., Rogledi, S., Torelli, L., 2003. Gravity Tectonics driven by Quaternary Uplift in the Northern Apennines: insights from the La Spezia-Reggio Emilia Geo-Transect. Quaternary International, 101/102, 13-26.

Bennett, R. A., Serpelloni, E., Hreinsdòttir, S., Brandon, M. T., Buble, G., Basic, T., Casale, G., Cavaliero, A., Anzidei, M., Marjonovic, M., Minelli, G., Molli, G., Montanari, A., 2012. Syn-convergent extension observed using the RETREATGPS network, northern Apennines Italy. J. Geophys. Res., 117, B04408.

Bertotti G., Capozzi R. and Picotti V., 1997, Extension controls Quaternary tectonics, geomorphology and sedimentation of the N-Apennines foothills and adjacent Po Plain (Italy), Tectonophysics, 282, 291-301.

Bigi, S., Cosentino, D., Parotto, M., Sartori, R., Scandone, P., 1991. Structural Model ofItaly. Scale 1: 500.000. C.N.R., Progetto Finalizzato Geodinamica, Selca, Florence,Italy.

Boccaletti, M., Corti, G., Martelli, L., 2011. Recent and active tectonics of the externalzone of the Northern Apennines (Italy). Int. J. Earth Sci., 100 (6), 1331-1348.

Boccaletti, M., Bonini, M., Corti, G., Gasperini, P., Martelli, L., Piccardi, L., Tanini, C.,Vannucci, G., 2004. Carta simotettonica della regione Emilia Romagna, 1:250.000e note illustrative, SELCA Editore, Firenze.

Bonini, L., Toscani, G., Seno S., 2014. Three-dimensional segmentation and different rupture behavior during the 2012 Emilia seismic sequence (Northern Italy). Tectonophysics, 630, 33-42.

Bormann, P. (Ed.), 2012. New Manual of Seismological Observatory Practice (NMSOP-2). IASPEI, GFZ German Research Centre for Geosciences, Potsdam; http://nmsop.gfz-

potsdam.de. DOI:10.2312/GFZ.NMSOP-2 urn:nbn:de:kobv:b103-NMSOP-2.

Burrato, P., Ciucci, F., Valensise, G., 2003. An inventory of river anomalies in the Po plain, Northern Italy: evidence for active blind thrust faulting. Annals of Geophysics, 46, 865-882.

Burrato, P., Vannoli, P., Fracassi, U., Basili, R., Valensise, G., 2012. Is blind faulting truly invisible? Tectonic-controlled drainage evolution in the epicentral area of the May 2012, Emilia-Romagna earthquake sequence (northern Italy). Annals of Geophysics, 55 (4), 525-531.

Carannante, S., Cattaneo, M., Marzorati, S., Monachesi, G., Spallarossa, D., 2012. "Sequenza Emilia 2012: modelli preliminari di propagazione e loro influenza sulla qualità delle localizzazioni, GNGTS proceedings, 31° national meeting, 2012 (in Italian).

Carminati, E., Scrocca, D., Doglioni, C., 2010. Compaction-induced stress variations with depth in an active anticline: Northern Apennines. Italy. J. Geophys. Res., 115, B02401.

Cattaneo, M., Augliera, P., Spallarossa, D., Eva, C., 1997. Reconstruction of a seismogenetic structure by multiplet analysis: an example of Western Liguria, Italy,. Bull. Seism. Soc. Am., 87, 971-986.

Chiarabba, C., Jovane, L., Di Stefano, R., 2005. A new view of Italian seismicity using 20 years of instrumental recordings. Tectonophysics, 395, 251-268.

Chiarabba, C., De Gori, P., Improta, L., Lucente, F. P., Moretti, M., Govoni, A., Di Bona, M.,

Margheriti, L., Marchetti, A., Nardi, A., 2014. Frontal compression along the Apennines thrust system: The Emilia 2012 example from seismicity to crustal structure. J. Geodyn., 82, 98-109.

Ciaccio, M. G., Chiarabba, C., 2002. Tomographic models and seismotectonics of the Reggio-Emilia region, Italy.Tectonophysics, 344, 261-276.

Cooper, M. A., Williams, G. D., de Graciansky, P. C., Murphy, R. W., Needham, T., de Paor, D., Stoneley, R., Todd, S. P., Turner, J. P., Ziegler, P. A., 1989. Inversion Tectonics - a discussion. Geological Society, London, Special Publications 1989, vol. 44, 335-347.

D'Alessandro A., Luzio D., D'Anna G., Mangano, G., 2010. Valutazione della performance di localizzazione della RSNC-INGV tramite simulazione numerica. Quaderni di Geofisica INGV,, n. 83.

Eberhart-Phillips, D., 1986. Three-dimensional velocity structure in Northern California coast ranges from inversion of local earthquake arrival times. Bull. Seismol. Soc. Am., 76, 1025-1052.

Fantoni, R., Franciosi, R., 2010. Tectono-sedimentary setting of the Po Plain and Adriatic foreland. Rend. Fis. Acc. Lincei, 21, S197-S209, http://dx.doi.org/10.1007/s12210-010-0102-4.

Fantoni, R., Franciosi, R., 2008. 8 geological sections crossing Po Plain and Adriatic foreland. Rend. online Soc. Geol. It., 3, 365-366.

Frémont, M. J., Malone, S. D., 1987. High precision relative locations of earthquakes at Mount St. Helens, Washington. J. Geophys. Res., 92, 10,223-10,236.

Ghielmi, M., Minervini, M., Nini, C., Rogledi, S., Rossi, M., Vignolo, A., 2010. Sedimentary and tectonic evolution in the eastern Po Plain and northern Adriatic Sea area from Messinian to Middle Pleistocene (Italy). In: Sassi, F.P. (Ed.), Nature and Geodynamics of the Lithostere in Northern Adriatic. Rend. Fis. Acc. Lincei, 21 (Suppl. 1), 131-166.

Ghielmi, M., Minervini, M., Nini, C., Rogledi, S., Rossi, M., 2013. Late Miocene–Middle Pleistocene sequences in the Po Plain—Northern Adriatic Sea (Italy): the stratigraphic record of modification phases affecting a complex foreland basin. Mar. Pet. Geol., 42, 50-81.

Gomberg, J. S., Shedlock, K. M., Roecker, S. W., 1990. The effect of S-Wave arrival times on the accuracy of hypocenter estimation. Bull. Seism. Soc. Am., 80, 1605-1628.

Got, J.-L., Fréchet, J., Klein, F. W., 1994. Deep fault plane geometry inferred from multiplet relative relocation beneath the south flank of Kilauea. J. Geophys. Res., 99, 15,375-15,386.

Govoni, A., Marchetti, A., De Gori, P., Di Bona, M., Lucente, F. P., Improta, L., Chiarabba, C., Nardi, A., Margheriti, L., Piana Agostinetti, N., Di Giovambattista, R., Latorre, D., Anselmi, M., Ciaccio, M. G., Moretti, M., Castellano, C., Piccinini, D., 2014. The 2012 Emilia seismic sequence (Northern Italy): imaging the thrust fault system by accurate aftershocks location. Tectonophysics, 622, 44-55.

Hanks, T. C., 1975. Strong ground motion of the San Fernando, California, earthquake: ground displacements. Bull. Seisrn. Soc. Am., 65, 193-225.

Haslinger, F., 1998. Velocity structure, seismicity and seismotectonics of northwestern Greece between the Gulf of Arta and Zakynthos, PhD thesis, ETH Zurich, Zurich, 176 p.

Hisada, Y., Aki, K., Teng, T.-L., 1993. 3-D simulations of the surface wave propagation in the Kanto sedimentary basin, Japan (Part 2: Application of the surface wave BEM). Bull. Seism. Soc. Am., 83, 1700-1720.

Joyner, W. B., 2000. Strong motion from surface waves in deep sedimentary basins. Bull. Seism. Soc. Am., 90, S95-S112.

Kagawa, T., Zhao, B., Miyakoshi, K., Irikura, K., 2004. Modeling of 3-D basin structures for seismic wave simulations based on available information on the target area: Case study of the Osaka Basin, Japan. Bull. Seism. Soc. Am., 94, 1353-1368.

Kissling, E., S. Husen, and F. Haslinger, Model parameterization in seismic tomography: A choice of consequences for the solution quality, Phys. Earth Planet. Inter., 123, 89–101, 2001.

Lahr, J. C., 1979. HYPOELLIPSE: A computer program for determining local earthquake hypocentral parameters, magnitude, and first motion pattern. U.S. Geol. Surv. Open File Rep., 79-431, 310 pp.

Lavecchia, G., De Nardis, R., Cirillo, D., Brozzetti, F., Boncio, P., 2012. The May–June2012

Ferrara arc earthquakes (northern Italy): structural control of the spa-tial evolution of the seismic sequence and of the surface pattern of coseismicfractures. Annals of Geophysics, 55 (4), 533- 540

Luzi, L., Pacor, F., Ameri, G., Puglia, R., Burrato, P., Massa, M., Augliera, P., Franceschina, G., Lovati, S., Castro, R., 2013. Overview on the strong-motion data recorded during the May-June 2012 Emilia seismic sequence. Seismological Research Letters, 84, 4, 629-644.

Malagnini, L., Herrmann, R. B., Munafò, I., Buttinelli, M., Anselmi, M., Akinci, A., Boschi, E., 2012. The 2012 Ferrara seismic sequence: Regional crustal struc-ture, earthquake sources, and seismic hazard. Geophys. Res. Lett., 39, L19302.

Marshak, S., Karlstrom, K., Timmons, J. M., 2000. Inversion of Proterozoic extensional faults: an explanation for the pattern of Laramide and Ancestral Rockies intracratonic deformation, United States. Geology, 28, 735-738.

Marzorati, S., Carannante, S., Cattaneo, M., D'Alema, E., Frapiccini, M., Ladina, C., Monachesi, G., 2012. Emergenza sismica 2012 in Emilia Romagna: attività sperimentali di supporto alla rete sismica mobile INGV svolte dal personale della sede di Ancona. Rapporti Tecnici INGV, 236, ISSN 2039-7941.

Marzorati, S., Massa, M., Cattaneo, M., Monachesi, G., Frapiccini, M., 2014. Very detailed seismic pattern and migration inferred from the April 2010 Pietralunga (northern Italian Apennines) micro-earthquake sequence. Tectonophysics, 610, 91-109.

Massa, M., Eva, E., Spallarossa, D., Eva, C., 2006. Detection of earthquake clusters on the basis of waveforms similarity: an application in the Monferrato region (Piemonte, Italy). Journal of seismology, vol. 10, 1-22.

Massa, M., Augliera, P., 2013. Teleseisms as estimator of experimental long period site amplifications: example in the Po Plain (Italy) from the 2011, Mw 9.0, Tohoku-Oki (Japan) earthquake. Bulletin Seismological Society of America, vol. 103, n. 5, 2541–2556.

Michelini, A., Lomax, A., 2004. The effect of velocity structure errors on double-difference earthquake location. *Geophys. Res. Lett.*, 31, L09602.

Moretti, M., Abruzzese, L., Abu Zeid, N., Augliera, P., Azzara, R., Barnaba, C., Benedetti, L., Bono, A., Bordoni, P., Boxberger, T., Bucci, A., Cacciaguerra, S., Calò, M., Cara, F., Carannante, S., Cardinale, V., Castagnozzi, A., Cattaneo, M., Cavaliere, A., Cecere, G., Chiarabba, C., Chiaraluce, L., Ciaccio, M. G., Cogliano, R., Colasanti, G., Colasanti, M., Cornou, C., Courboulex, F., Criscuoli, F., Cultrera, G., D'Alema, E., D'Ambrosio, C., Danesi, S., De Gori, P., Delladio, A., De Luca, G., Demartin, M., Di Giulio, G., Dorbath, C., Ercolani, E., Faenza, L., Falco, L., Fiaschi, A., Ficeli, P., Fodarella, A., Franceschi, D., Franceschina, G., Frapiccini, M., Frogneux, M., Giovani, L., Govoni, A., Improta, L., Jacques, E., Ladina, C., Langlaude, P., Lauciani, V., Lolli, B., Lovati, S., Lucente, F.P., Luzi, L., Mandiello, A., Marcocci, C., Margheriti, L., Marzorati, S., Massa, M., Mazza ,S., Mercerat, D., Milana ,G., Minichiello, F., Molli, G., Monachesi, G., Morelli, A., Moschillo, R., Pacor, F., Piccinini, D., Piccolini, U., Pignone, M., Pintore, S., Pondrelli, S., Priolo, E., Pucillo, S., Quintiliani, M., Riccio, G., Romanelli, M., Rovelli, A., Salimbeni, S., Sandri, L., Selvaggi, G., Serratore, A., Silvestri, M., Valoroso, L., Van der Woerd, J., Vannucci, G., Zaccarelli, L., 2012. Rapid-

response to the earthquake emergency of May 2012, in the Po Plain, Northern Italy. Annals of Geophysics, 55, 4, 583-590.

Patacca, E., Scandone, P., Di Luzio, E., Cavinato, G. P., Parotto, M., 2008. Structural architecture of the central Apennines: Interpretation of the CROP 11 seismic profile from the Adriatic coast to the orographic divide. Tectonics 27, TC3006, http://dx.doi.org/10.1029/2005TC001917.

Payton, C. E., (Ed.), 1977. Seismic Stratigraphy-Application to Hydrocarbon Exploration: American Association of Petroleum Geologists Memoir 26, 516 p.

Pezzo, G., Merryman, J. P., Tolomei, C., Salvi, S., Atzori, S., Antonioli, A., Trasatti, E., Novali, F., Serpelloni, E., Candela, L., Giuliani, R., 2013. Coseismic deformation and source modeling of the May 2012 Emilia (Northern Italy) earthquakes. Seism. Res. Lett., 84, 645–655.

Pfiffner, A., 2006. Thick-skinned and thin-skinned styles of continental contraction. Geological Society of America Special Papers 2006, 414, 153-177.

Picotti, V., Pazzaglia, F. J., 2008. A new active tectonic model for the construction of the Northern Apennines mountain front near Bologna (Italy). J. Geophys. Res., 113, B08412.

Pieri, M., Groppi, G., 1981. Subsurface geological structure of the Po Plain, Italy, in Progetto Finalizzato Geodinamica, edited by C.N.R., Publ. N° 414.

Pieri M., 1983, Three seismic profiles through the Po Plain, A.A.P.G., Studies in Geology, Series 15, (3), 3.4.1, 8-26

Poupinet, G., Ellsworth, W. L., Frechet, J., 1984. Monitoring velocity variations in the crust using earthquake doublets: An application to the Calaveras Fault California. J. Geophys. Res., 89, 5719- 5731.

Rao, S., Salvaterra, L., Acerra, C., 2010. Software per l'installazione e la configurazione della stazione sismica GAIA2. Rapporti Tecnici INGV, 130, 52 p. (in Italian).

Rovida A., Camassi R., Gasperini P. e Stucchi M., 2011. CPTI11, la versione 2011 del Catalogo Parametrico dei Terremoti Italiani. Milano, Bologna, (in Italian) http://emidius.mi.ingv.it/CPTI, DOI: 10.6092/INGV.IT-CPTI11

Sato, T., Graves, R. W., Somerville, P. G., 1999. Three-dimensional finite-difference simulations of long-period strong motions in the Tokyo metropolitan area during the 1990 Odawara earthquake (MJ 5.1) and the great 1923 Kanto earthquake (MS 8.2) in Japan. Bull. Seismol. Soc. Am., 89, 579-607.

Scognamiglio, L., L. Margheriti, F. M. Mele, E. Tinti, A. Bono, P. De Gori, V. Lauciani, F. P. Lucente, A. G. Mandiello, C. Marcocci, S. Mazza, S. Pintore, and M. Quintiliani, 2012. The 2012 Pianura Padana Emiliana Seimic Sequence: Locations and Magnitudes. Annals of Geophysics, "The Emilia (northern Italy) seismic sequence of May-June, 2012: preliminary data and results", Anzidei M., Maramai A. and Montone P. (Eds), 55, 4, 10.4401/ag-6159

Scrocca, D., Carminati, E., Doglioni, C., Marcantoni, D., 2007. Slab retreat and active shortening along the Central-Northern Apennines. In: Lacombe O, Lavq J, Roure F, Verges J (eds) Thrust belts and Foreland Basins: from fold kinematics to hydrocarbon systems. Frontier in Earth Sciences, Springer, 471–487.

Shaw, J.H. and Suppe, J., 1994. Active faulting and growth folding in the eastern Santa Barbara Channel, california. Geological Society of America, Bulletin, 106, 607-626.

Somerville, P. G., Collins, N. F., Graves, R. W.,Pitarka, A., 2004. An engineering ground motion model for basin generated surface waves, Proc. 13th World Conference on Earthquake Engineering, Vancouver, Canada, Paper 515.

Spallarossa, D., Ferretti, G., Scafidi, D., Pasta, M., 2011. Picking automatico nella rete sismica dell'Italia Nord-Occidentale (RSNI). In Cattaneo M. e Moretti M., (eds). Monitoraggio sismico del territorio nazionale: stato dell'arte e sviluppo delle reti di monitoraggio sismico. Miscellanea INGV 2011, 10, pp. 141-146 (in Italian).

Stein, R. S., Yeats, R. S., 1989. Hidden Earthquakes, Sci. Am., 260, 48-57.

Stucchi, M., Meletti, C., Montaldo, V., Crowley, H., Calvi, G.M., Boschi, E., 2011. Seismic hazard assessment (2003-2009) for the Italian building code. Bull. Seismol. Soc. Am., 101, 4, 1885-1911.

Stucchi, M., Rovida, A., Gomez Capera, A. A., Alexandre, P., Camelbeeck, T., Demircioglu, M. B., Gasperini, P., Kouskouna, V., Musson, R. M.W., Radulian, M., Sesetyan, K., Vilanova,

S., Baumont, D., Bungum, H., Faeh, D., Lenhardt, W., Makropoulos, K., Martinez Solares, J. M., Scotti, O., Živčić, M., Albini, P., Batllo, J., Papaioannou, C., Tatevossian, R., Locati, M., Meletti, C., Viganò, D., Giardini, D., 2012. The SHARE European Earthquake Catalogue (SHEEC) 1000-1899. Journal of Seismology, 17, 2, 523-544.

Thurber, C. H., 1983. Earthquake locations and three-dimensional crustal structure in the Coyote Lake area, central California. J. Geophys. Res., 88, 8226-8236.

Thurber, C.H., 1993. Local earthquake tomography: velocities and Vp/Vs – theory, In: H.M. Iyer and K. Hirahara (eds.), Seismic Tomography: Theory and Practice. Chapman & Hall, 842 pp.

Tizzani, P., Castaldo, R., Solaro, G., Pepe, S., Bonano, M., Casu, F., Manunta, M.,Manzo, M., Pepe, A., Samsonov, S., Lanari, R., Sansosti, E., 2013. New insights into the 2012 Emilia (Italy) seismic sequence through advanced numerical modeling of ground deformation InSAR measurements. Geophys. Res. Lett., 40, 1971–1977.

Toscani, G., Burrato, P., Di Bucci, D., Seno, S., Valensise, G., 2009. Plio-Quaternary tec-tonic evolution of the northern Apennines thrust fronts (Bologna-Ferrara sectionItaly): seismotectonic implications. Boll. Soc. Geol. Italiana Servizio Geol. d'Italia (Italian J. Geosci.), 128, 605-613.

Um, J., Thurber, C. H., 1987. A fast algorithm for two-point seismic ray tracing. Bull. Seismol. Soc. Am., 77, 972–986.

Ventura, G., Digiovambattista, R., 2013. Fluid pressure, stress field and propagation style of coalescing thrusts from the analysis of the 20 May 2012 ML 5.9 Emilia earthquake (Northern Apennines, Italy). Terra Nova, 25, 72-78.

Waldhauser, F., Ellsworth, W. L., 2000. A double-difference earthquake location algorithm: Method and application to the northern Hayward fault. Bull. Seism. Soc. Am., 90, 1353-1368.

Waldhauser, F., 2001. HypoDD: A computer program to compute double-difference hypocenter locations. U.S. Geol. Surv. open-file report, 01-113, Menlo Park, California.

Figure captions

Figure 1. (a) May-June 2012 Emilia earthquakes (Po Plain, northern Italy) as provided by the INGV bulletin (~ 2,150 epicenters) soon after the sequence (http://iside.rm.ingv.it). Violet circles, May 20 and 29 mainshocks; red, aftershocks with $M_L \geq 5.0$; green: aftershocks with $4.0 \leq M_L < 5.0$; triangles, INGV permanent (gray) and temporary (white) seismic stations; gray lines, ray paths. **(b)** Simplified structural map of the Northern Apennines (after Argnani et al., 2003). 1, metamorphic complex; 2, main blind thrust fronts: a, external front; b, front of the Mesozoic carbonates; c, 'basement' front; 3, isochrons of the top of the 'basement', in seconds (TWT).

Figure 2. Instrumental **(a)** and historical **(b)** seismicity of the area up to May 15, 2012.

Figure 3. (a) Distributions of rms and horizontal (erh) and vertical (erz) errors, referred to the high quality dataset of 650 events used to calibrate the new 1D and 3D velocity models. Data were selected starting from the preliminary locations, obtained using the INGV (1D) three-layer velocity model routinely used for the first locations (D'Alessandro et al., 2010). (b) The new P-wave , S-wave and Vp/Vs ratio, as 1D velocity models

Figure 4. (a) Distribution of the Resolution Diagonal Elements (RDE). (b) Distribution of the Derivative Weighted Sum (DWS). White circles, relocated hypocenters, projected on the single layer with a range of ±2 km in depth; yellow stars, earthquakes with ML >5.0; red stars, May 20 and 29 mainshocks.

Figure 5. Spread Function Distribution (SF) and 70% smearing contour of the Vp model.

Black and gray crosses and contours, nodes with SF ≤1.5 and SF ≤2.0, respectively; red star, orange star, May 20 and 29 mainshocks, respectively. As the mainshocks are locate at halfway depths between the resolved layers, for greater accuracy, the events are projected onto the layer immediately below the depth of the location and on that immediately above.

Figure 6. Vp (a) and Vp/Vs (b) models represented as absolute values. Circles, relocated hypocenters, as described in Figures 6 and 7; yellow stars, earthquakes with ML >5.0; red stars, May 20 and 29 mainshocks; red lines, main thrusts of the Ferrara Arc; green lines, Mesozoic extensional faults.

Figure 7. Rms and horizontal (erh) and vertical (erh) error distributions. Continuous black line histograms refer to the preliminary dataset; gray histograms show the final distributions, after the accurate relocation step.

Figure 8. Map projection (a) and depth projections (b) of the :

1) ~ 2,150 INGV first locations (light grey circles) as provided soon after the sequence by the ISIDE (Italian Seismological Instrumental and Parametric database) bulletin (http://iside.rm.ingv.it);

2) 5,369 relocated events (dark green circles) obtained using the new 3D velocity model;

3) 1,300 relative located events selected on the basis of the rms (≤ 0.15 s) obtained from the absolute relocation.

Red and yellow stars indicate the seven events with ML >5 (in red the two mainshocks) that occurred during the Emilia sequence. The symbol sizes are proportional to their ML.

Figure 9. Map projection (a) and depth projections (b) of the 5,369 relocated earthquakes, as

a function of the time of occurrence.

Figure 10.

(a)

Top: simplified structural map of the Ferrara Arc showing the thrust fronts where the Mesozoic units are involved (black lines with triangles) and the Mesozoic extensional faults (gray lines), with the 2012 earthquakes shown. Thick gray lines labelled a, b, c, traces of cross sections shown on the right panels; grey circles, events with ML >3; yellow stars, events with ML >5; red stars, mainshocks of the May 20 and 29, 2012 Emilia sequence. Note that the belt of the Mesozoic extensional faults is wider just west of Ferrara, in the area of the 20 May, 2012, Emilia seismic sequence.

Middle and bottom: conversion of hypocentral depths into two-way travel time [TWT] in order to locate seismicity on the time migrated seismic profiles (right hand panels) with associated errors. Green point twt values evaluated using the new 1D local model (Fig. 3); blue point values obtained using the velocity log from a deep well located west of Ferrara.

(b)

Line drawings of the seismic profiles that cross the Ferrara Arc, from the location of profiles shown on left side of the panel . The Po Plain prograding unit is indicated by dotted pattern. Note how the 29 May seismicity follows the step in the carbonate units relatively closely, whereas the 20 May seismicity broadly defines a footwall shortcut trajectory with respect to the Mesozoic extensional fault. Length and breadth of the profiles b and c are indicated in the top panel of figure 10a.

Figure 11. The concept of the footwall shortcut (e.g., Cooper et al., 1989) as applied to the area of the May 20, 2012, mainshock (compare to Fig. 10, right panel c). As the deformation

affects the deeper crustal sectors, the re-activated Mesozoic extensional faults promote a footwall shortcut rupture, which folds the overlying Pliocene-Pleistocene detachment system that has a broader structural wavelength in the area of the Ferrara folds.

Figure 12. Interpretative tectonic sketches of the May 20 and 29, 2012, earthquakes. The seismicity distribution is broadly indicated by the gray pattern. The timing and space-pattern of deformation are indicated above each cross-section. **(a)** May 20 mainshock: the new rupture is given by an incipient shortcut fault located in the footwall of a major Mesozoic extensional fault. **(b)** May 29 mainshock: the seismicity is concentrated along the Mesozoic fault and is particularly well expressed in the Mirandola area. Both cases reflect the activation of a recent (post middle Pliestocene) deformation system (dashed bold lines), which is deeper than the Pliocene thrust system.

Table 1. The INGV seismic stations used in this study. Episensor (model: FBA-ES-T) is an accelerometer produced by Kinemetrics (http://www.kmi.com). GAIA2 is a low-cost INGV in-house-developed data-logger (Rao et al., 2010). For the other instruments see the websites http://www.nanometrics.ca (i.e.Trident, Taurus, Trillium 40s, Trillium 120s), www.reftek.com (i.e. Reftek-130) and www.lennartz-electronic.de (i.e. LE3D 5s and LE3Dlite 1s).

Table1
Click here to download Table: table1.xls

Foglio1

Code	Type	Latitude (°)	Longitude (°)	Altitude (m a.s.l.)	Digitizer	Accelerometer	Velocimeter
T0800	Temporary	44.8486	11.2479	9	TRIDENT	Episensor	Trillium 120s
T0802	Temporary	44.8750	11.1816	9	TAURUS	Episensor	/
T0803	Temporary	44.7668	11.35078	10	TAURUS	Episensor	/
T0805	Temporary	44.91872	11.32261	5	TAURUS	Episensor	/
T0811	Temporary	44.78367	11.22617	10	REFTEK-130	Episensor	LE3Dlite 1s
T0812	Temporary	44.95483	11.18117	7	REFTEK-130	Episensor	LE3Dlite 1s
T0813	Temporary	44.87783	11.19917	1	REFTEK-130	Episensor	LE3Dlite 1s
T0814	Temporary	44.79333	10.96917	16	REFTEK-130	Episensor	LE3Dlite 1s
T0815	Temporary	44.87300	11.71983	2	REFTEK-130	Episensor	LE3Dlite 1s
T0816	Temporary	44.72067	11.59750	1	REFTEK-130	Episensor	LE3Dlite 1s
T0817	Temporary	44.99167	11.45583	0	REFTEK-130	Episensor	LE3Dlite 1s
T0818	Temporary	44.93483	11.03033	5	REFTEK-130	Episensor	LE3Dlite 1s
T0819	Temporary	44.8873	10.8987	19	REFTEK-130	Episensor	LE3D 5s
T0820	Temporary	44.7912	11.5732	8	REFTEK-130	Episensor	LE3D 5s
T0821	Temporary	44.9035	11.5405	3	REFTEK-130	Episensor	LE3D 5s
T0822	Temporary	44.83282	11.3455	7	GAIA2	/	LE3Dlite 1s
T0823	Temporary	44.68617	11.27717	14	REFTEK-130	Episensor	LE3Dlite 1s
T0824	Temporary	44.75750	10.92750	72	REFTEK-130	Episensor	LE3Dlite 1s
T0825	Temporary	44.97297	10.84691	7	GAIA2	/	LE3D 5s
T0826	Temporary	44.83943	10.81133	13	GAIA2	Episensor	/
T0827	Temporary	44.93767	10.93183	11	REFTEK-130	Episensor	LE3Dlite 1s
T0828	Temporary	44.83083	10.91433	13	REFTEK-130	Episensor	LE3Dlite 1s
BDI	Permanent	44.06238	10.59698	830	TRIDENT	/	Trillum 40s
BRIS	Permanent	44.22454	11.76657	260	GAIA2	Episensor	Trillium 120s
CMPO	Permanent	44.5808	11.8056	2	GAIA2	Episensor	Trillum 40s

Figure1

Click here to download high resolution image

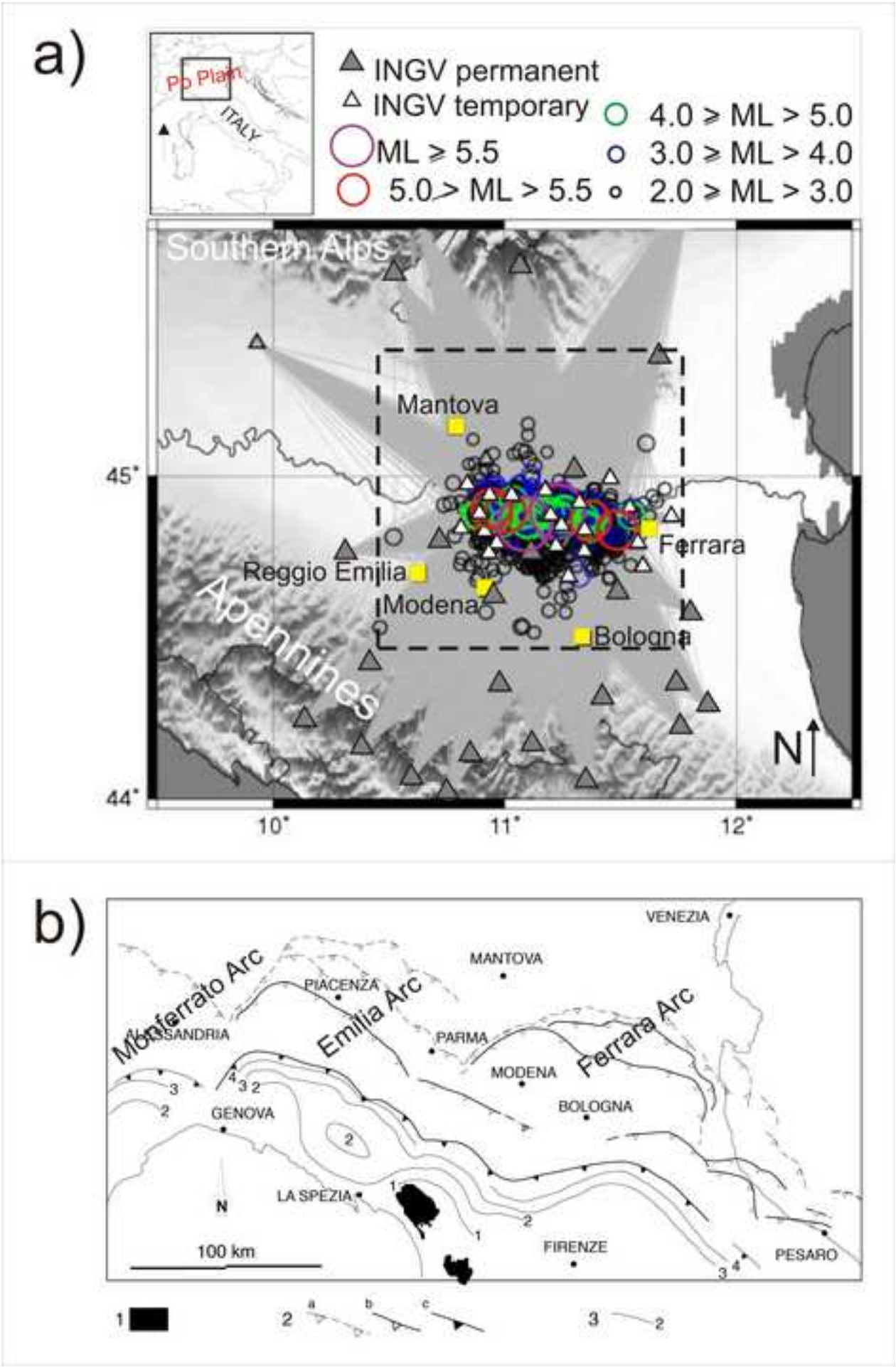

Figure2

Click here to download high resolution image

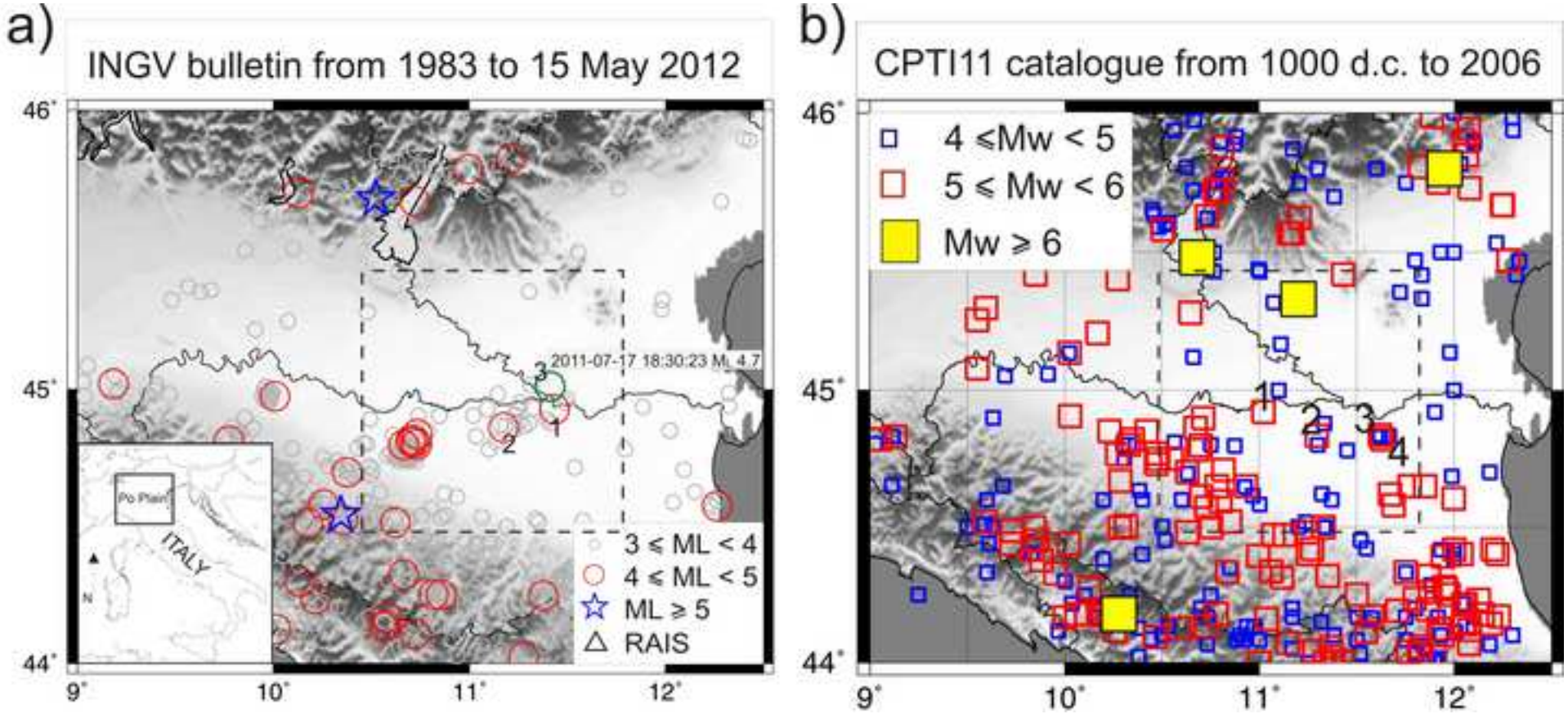

Figure3

Click here to download high resolution image

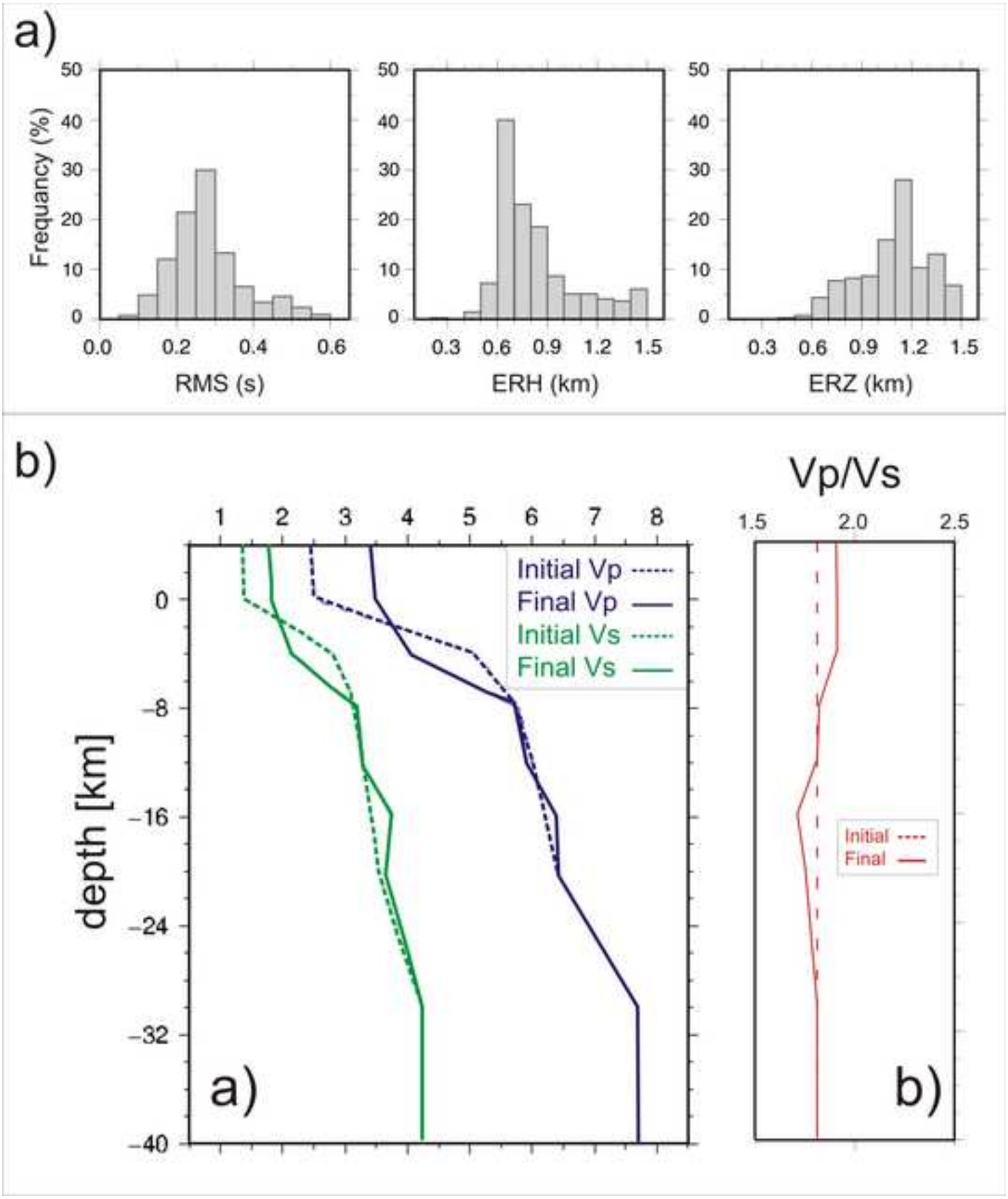

Figure4

Click here to download high resolution image

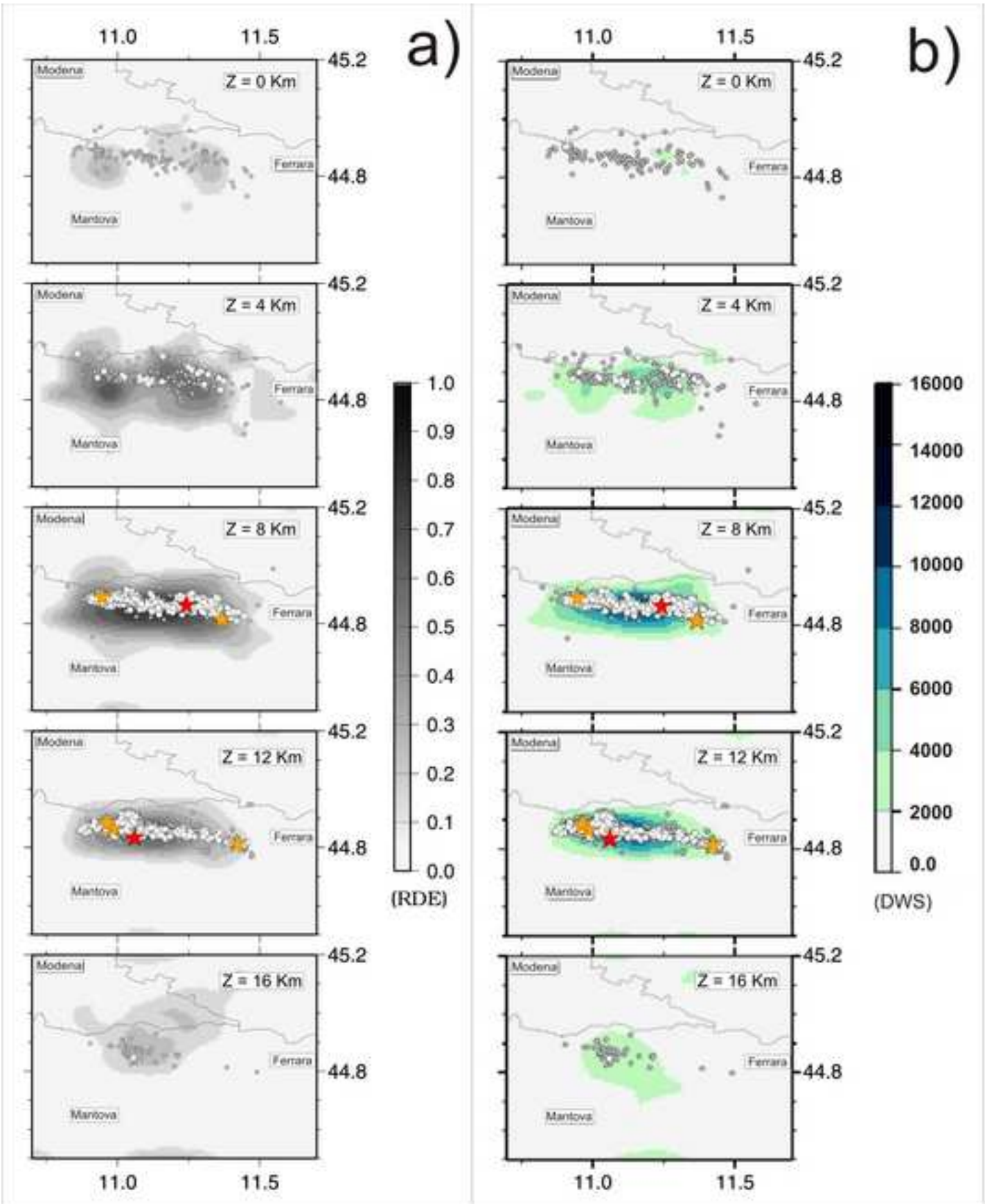

Figure5

Click here to download high resolution image

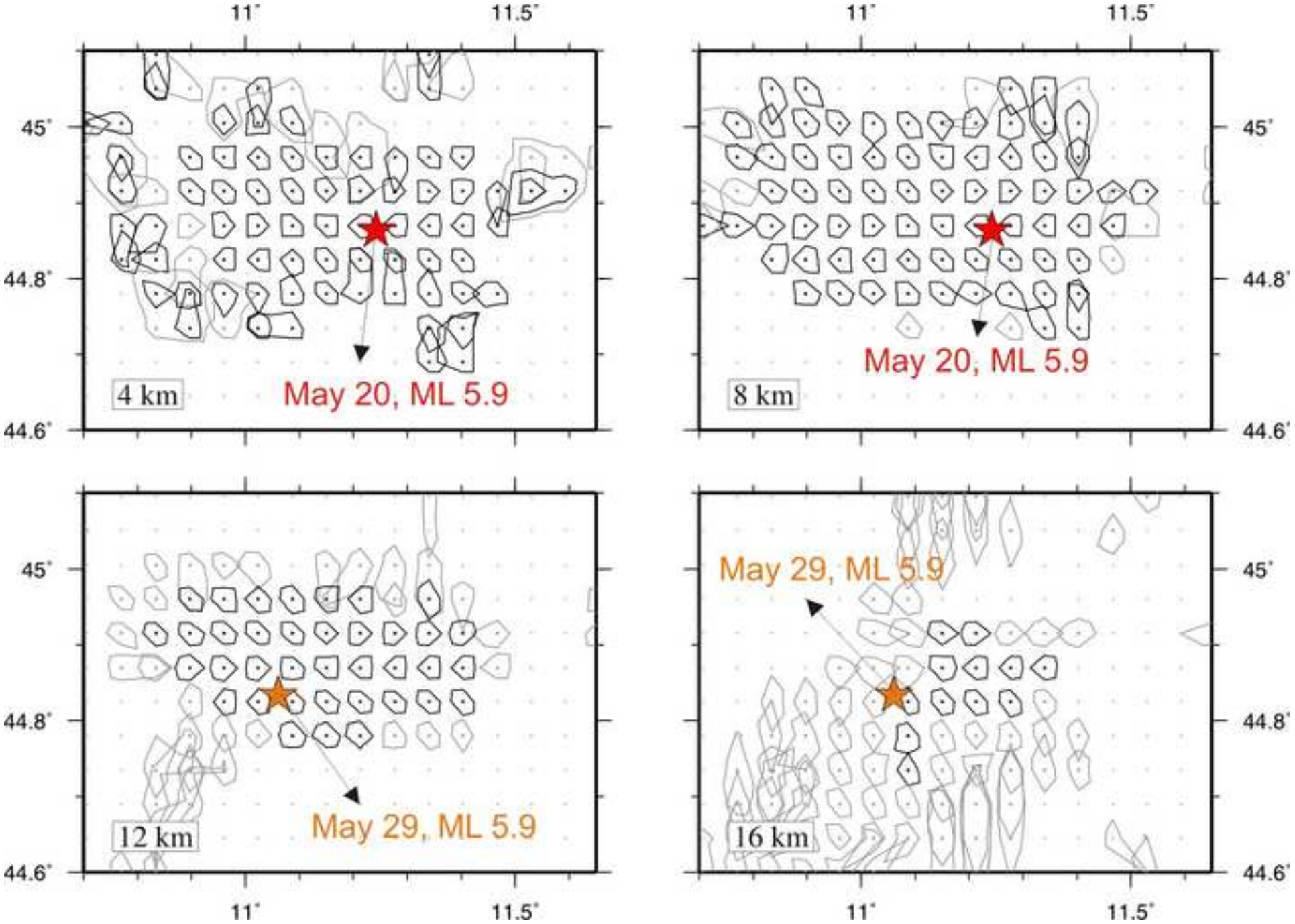

Figure6

Click here to download high resolution image

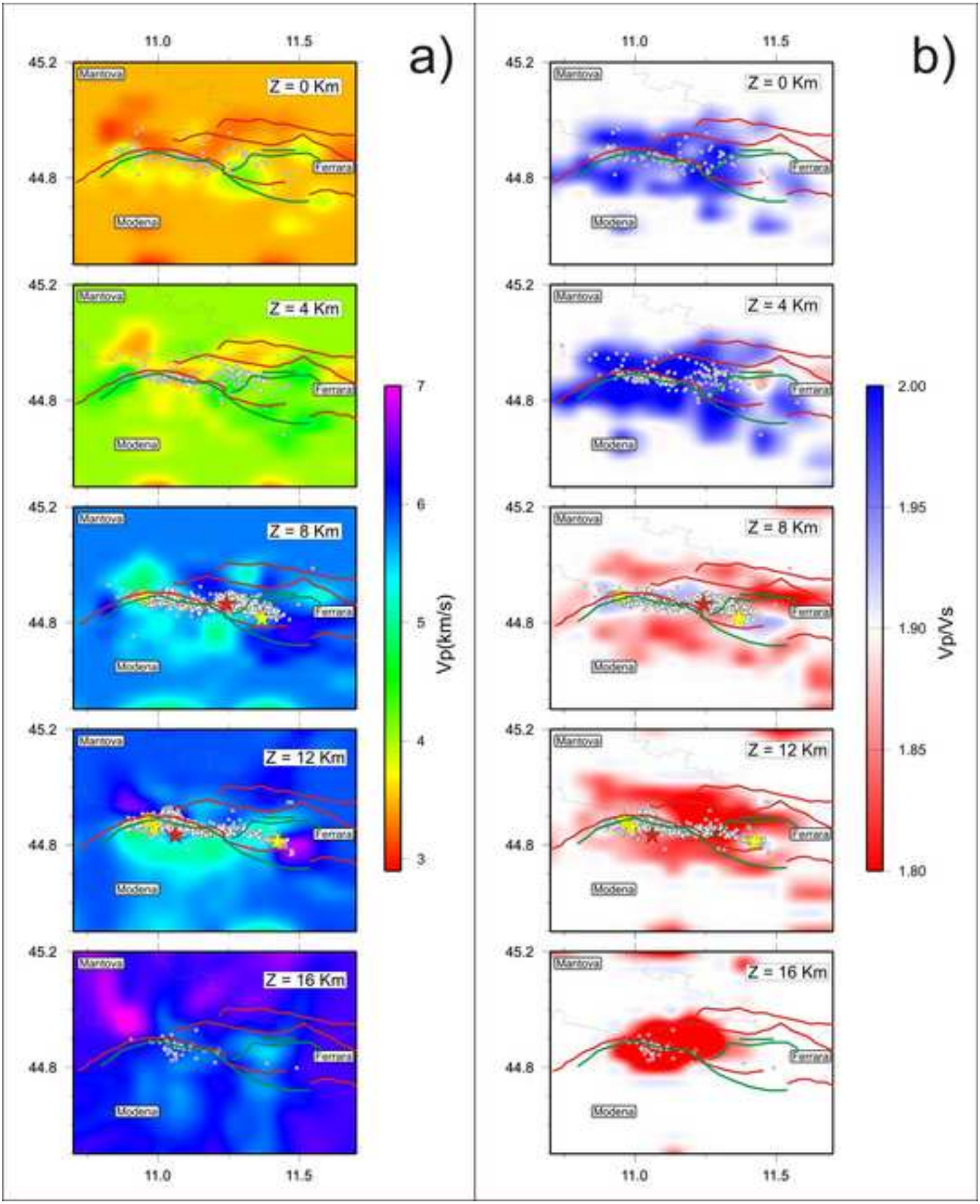

Figure7

Click here to download high resolution image

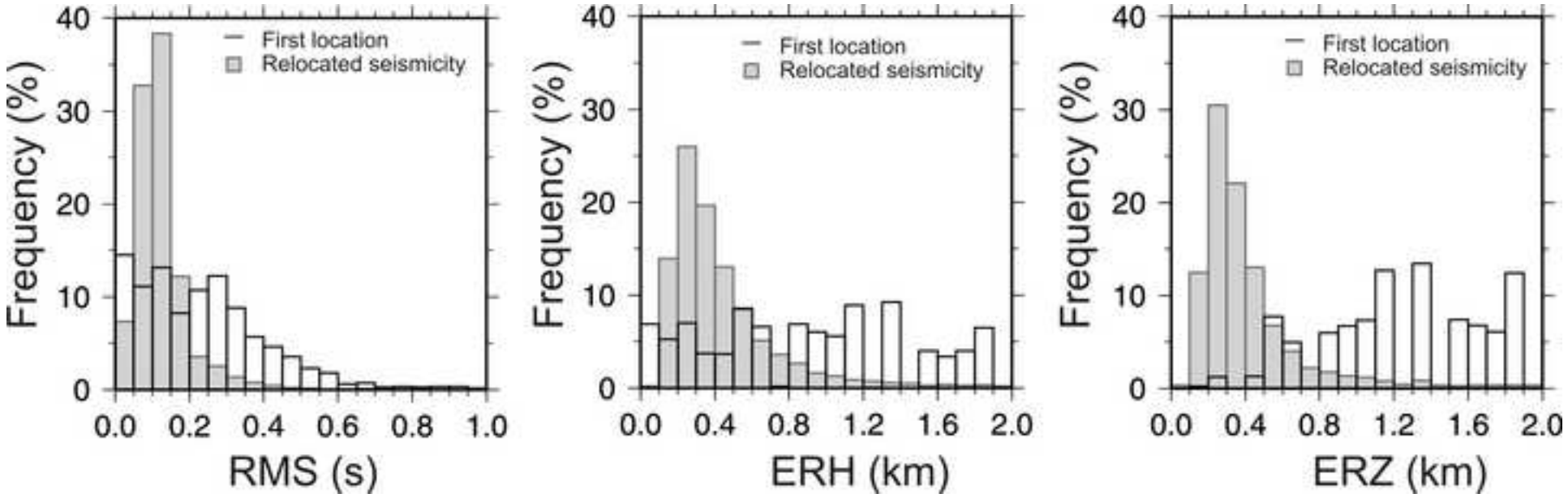

Figure8

Click here to download high resolution image

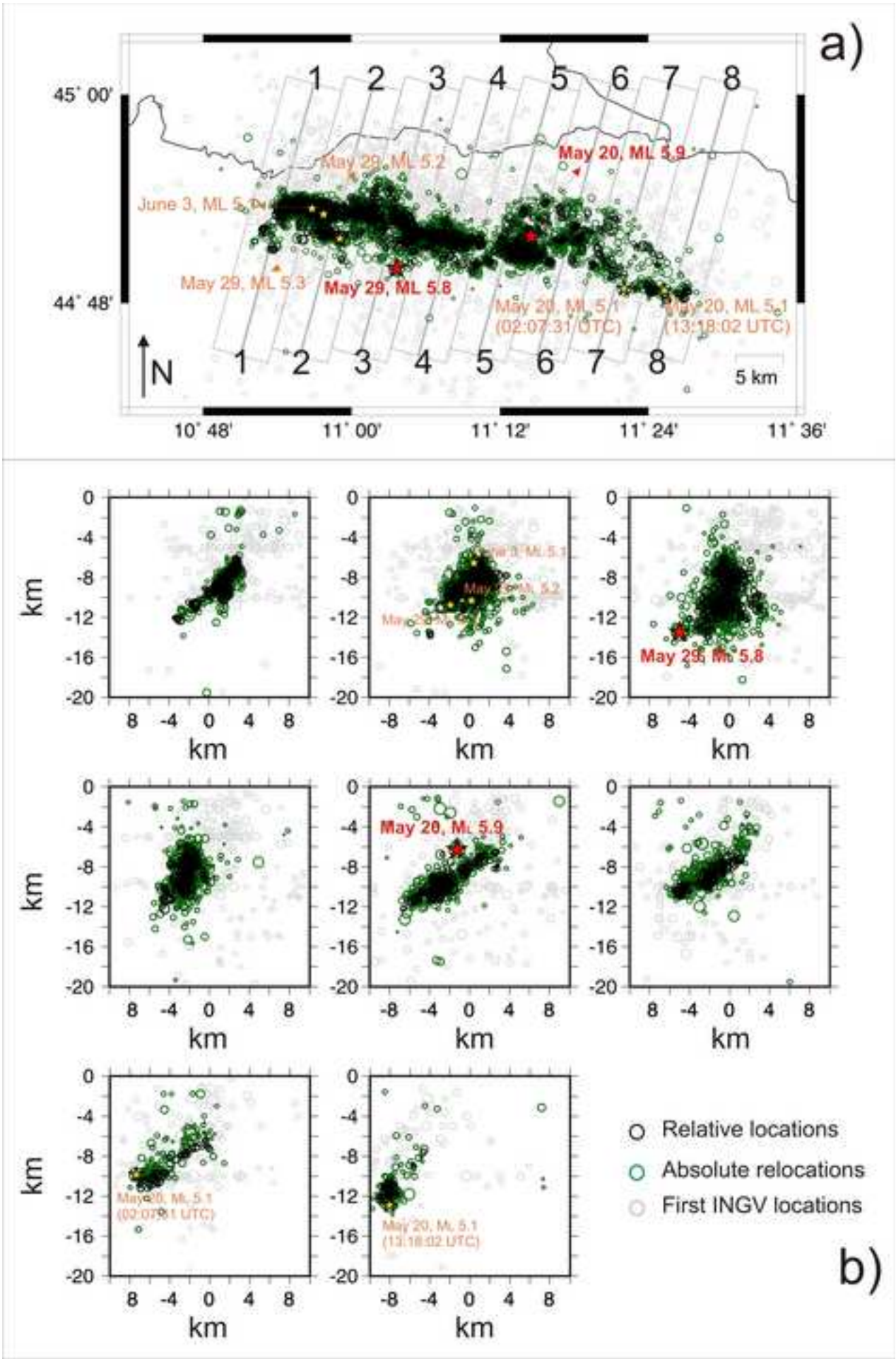

Figure9

Click here to download high resolution image

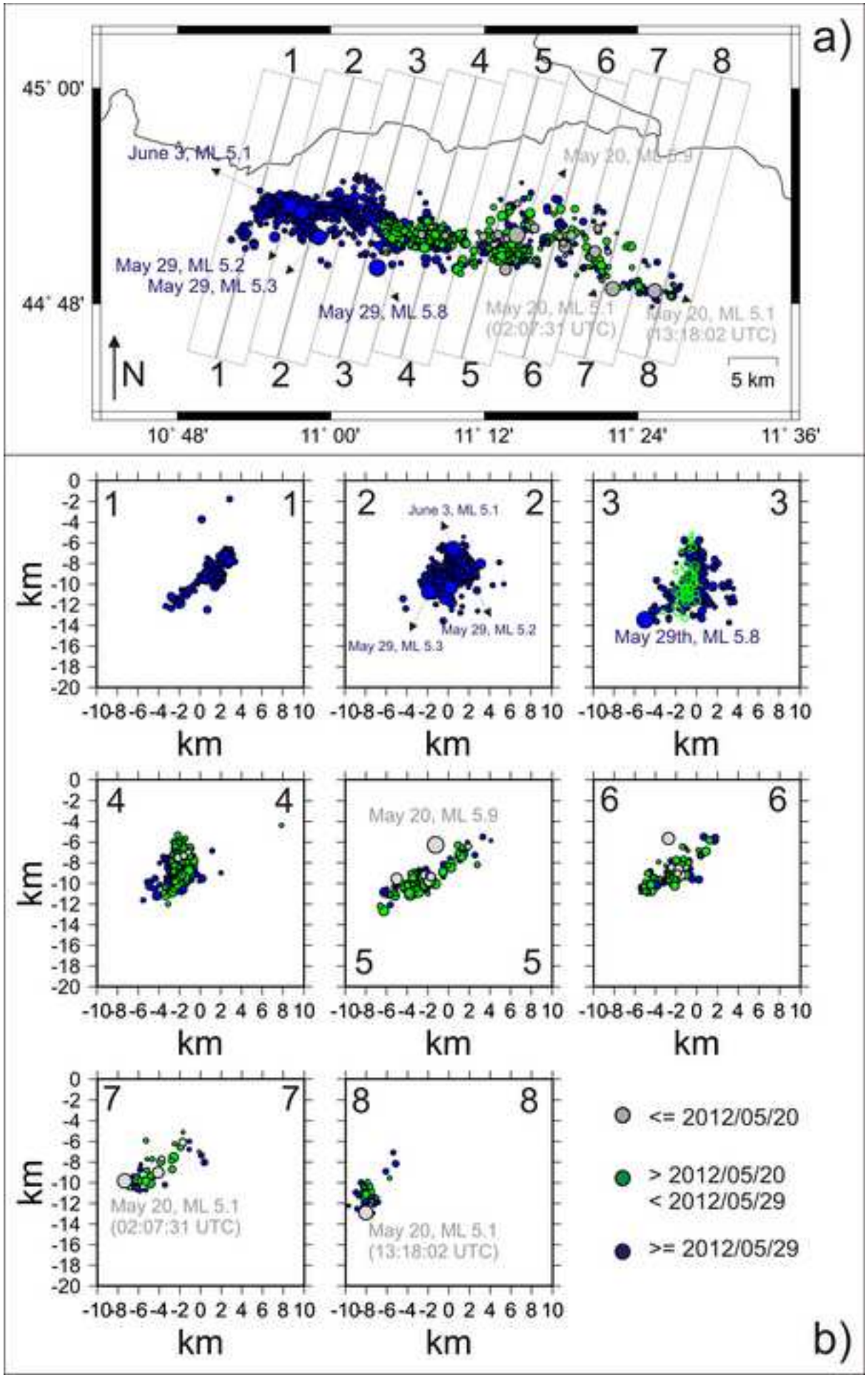

Figure10

Click here to download high resolution image

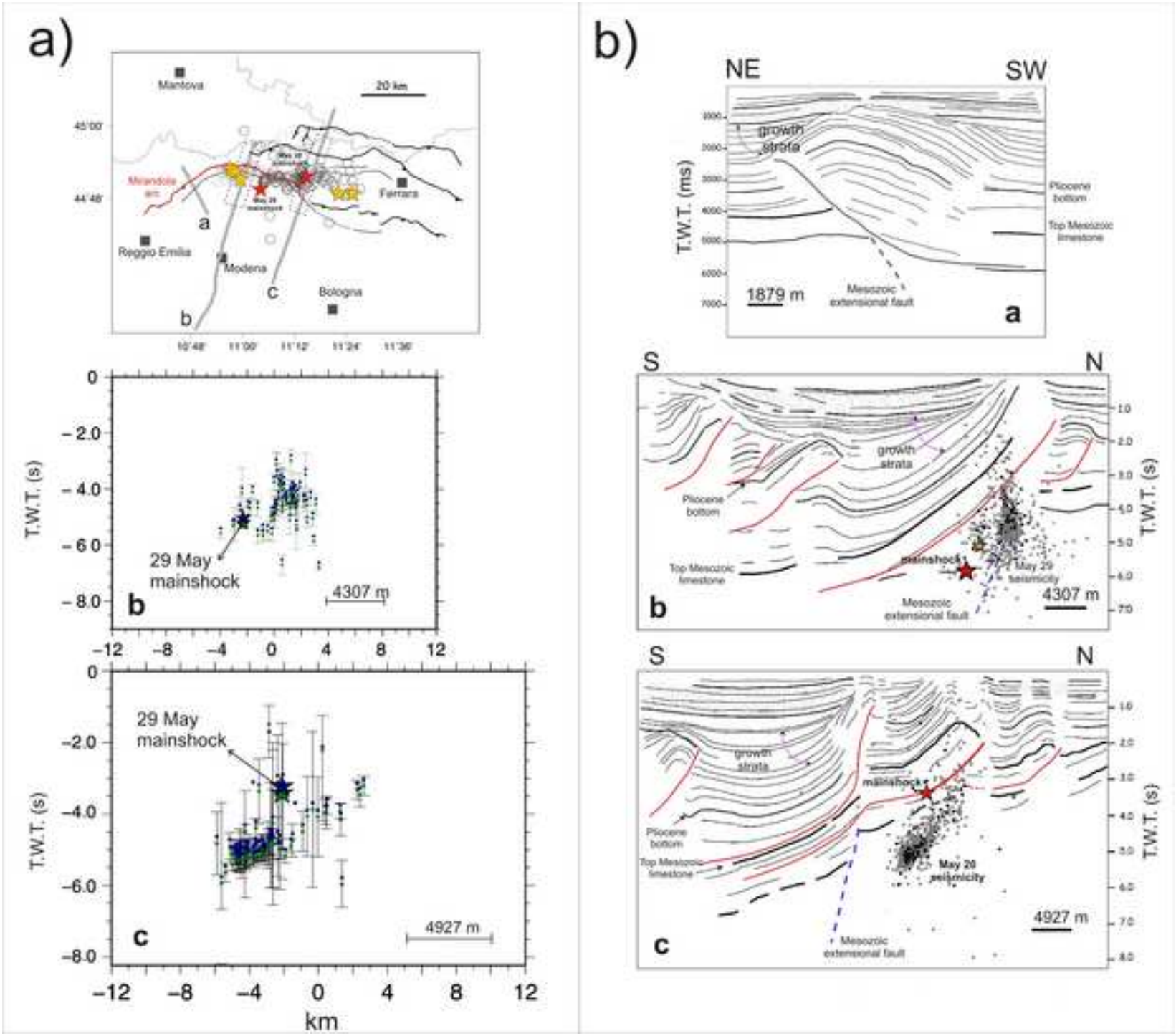

Figure11
Click here to download high resolution image

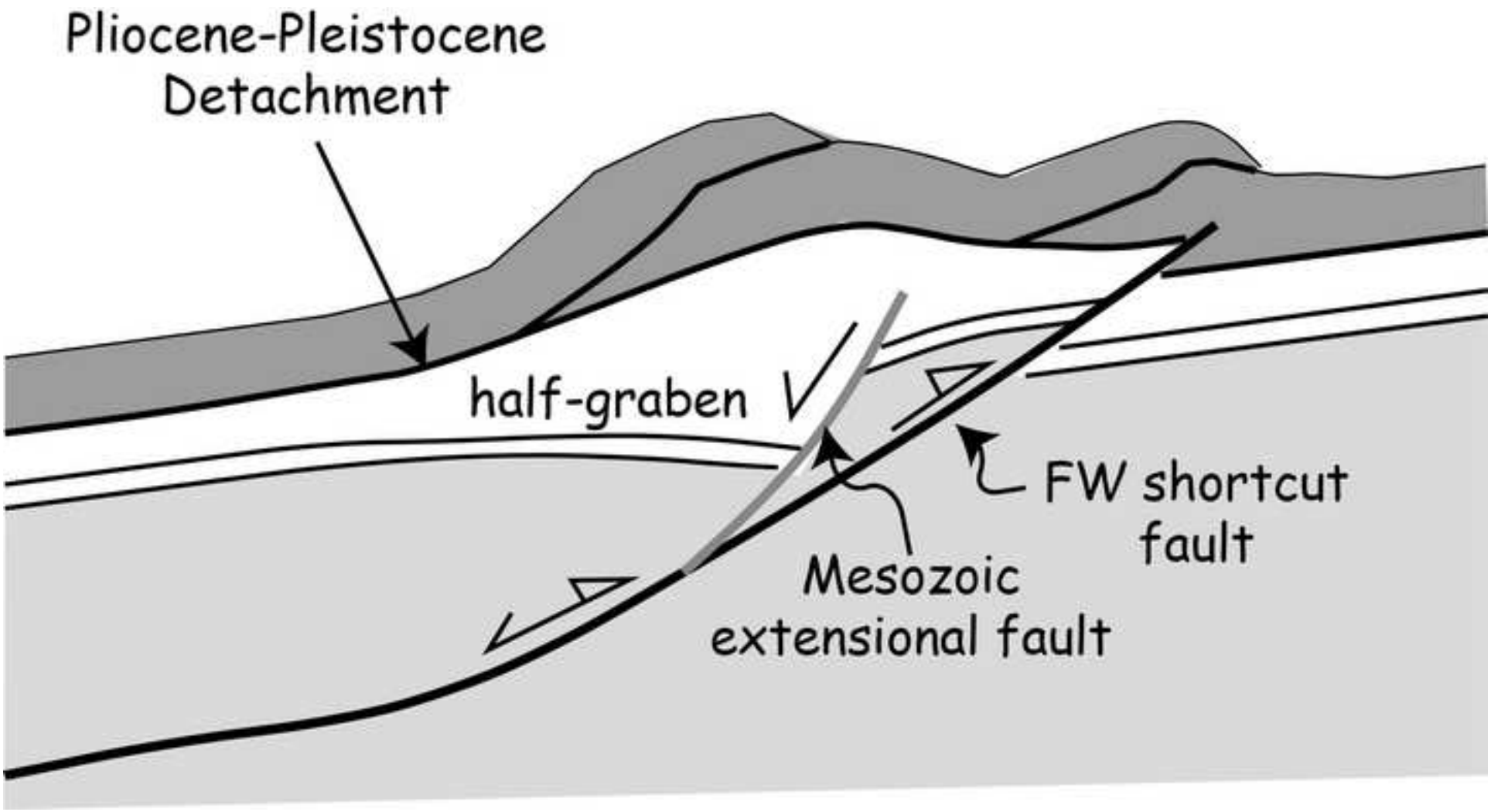

Figure12

Click here to download high resolution image